NAVAL POSTGRADUATE SCHOOL
MONTEREY, CALIFORNIA

THESIS

THREE DIMENSIONAL ACOUSTIC EFFECTS IN THE MIDDLE ATLANTIC BIGHT

by

Anthony F. D'Agostino

June, 1996

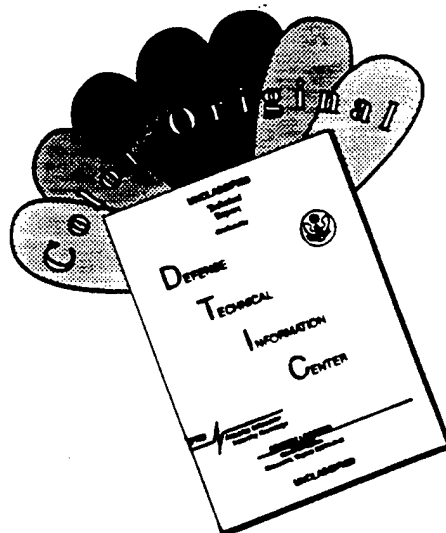Thesis Advisor: Ching-Sang Chiu
Thesis Co-Advisor: Kevin B. Smith

Approved for public release; distribution is unlimited.

19960930 036

DISCLAIMER NOTICE

THIS DOCUMENT IS BEST QUALITY AVAILABLE. THE COPY FURNISHED TO DTIC CONTAINED A SIGNIFICANT NUMBER OF COLOR PAGES WHICH DO NOT REPRODUCE LEGIBLY ON BLACK AND WHITE MICROFICHE.

REPORT DOCUMENTATION PAGE			Form Approved OMB No. 0704-0188

1. AGENCY USE ONLY *(Leave blank)*	2. REPORT DATE June 1996.	3. REPORT TYPE AND DATES COVERED Master's Thesis
4. TITLE AND SUBTITLE THREE DIMENSIONAL ACOUSTIC EFFECTS IN THE MIDDLE ATLANTIC BIGHT		5. FUNDING NUMBERS
6. AUTHOR(S) Anthony F. D'Agostino		
7. PERFORMING ORGANIZATION NAME(S) AND ADDRESS(ES) Naval Postgraduate School Monterey CA 93943-5000		8. PERFORMING ORGANIZATION REPORT NUMBER
9. SPONSORING/MONITORING AGENCY NAME(S) AND ADDRESS(ES)		10. SPONSORING/MONITORING AGENCY REPORT NUMBER
11. SUPPLEMENTARY NOTES The views expressed in this thesis are those of the author and do not reflect the official policy or position of the Department of Defense or the U.S. Government.		
12a. DISTRIBUTION/AVAILABILITY STATEMENT Approved for public release; distribution is unlimited.		12b. DISTRIBUTION CODE

13. ABSTRACT *(maximum 200 words)*

Under the sponsorship of the Office of Naval Research (ONR) PRIMER program, an integrated acoustic and oceanographic field experiment will be conducted jointly by the Naval Postgraduate School (NPS) and the Woods Hole Oceanographic Institution (WHOI) in the Middle Atlantic Bight (MAB) to study the propagation of sound from the continental slope to the continental shelf. In support of this field study the three-dimensional (3D) effects of the basic mean shelfbreak frontal thermal structure and sloping bathymetry on the planned tomography signal transmissions are modeled using ray methods. Both three-dimensional (3D) and two-dimensional (2D) ray paths and signal arrival structures for an upslope and cross-slope source-receiver geometry are simulated and compared. While the input sound speed field is from a previous summer-time hydrographic section, the input bathymetry is from a recently declassified U.S. Navy DBDB-0.5 data set. Significant 3D environmental effects are found in the modeled cross-slope transmissions, indicating that the physics of horizontal refraction and out-of-the-vertical-plane scattering will be required to properly analyze the acoustic measurements and to construct accurate tomographic maps.

14. SUBJECT TERMS Acoustic Tomography, Ocean Acoustics, Oceanography			15. NUMBER OF PAGES 53
			16. PRICE CODE
17. SECURITY CLASSIFICATION OF REPORT Unclassified	18. SECURITY CLASSIFICATION OF THIS PAGE Unclassified	19. SECURITY CLASSIFICATION OF ABSTRACT Unclassified	20. LIMITATION OF ABSTRACT UL

THREE DIMENSIONAL ACOUSTIC EFFECTS IN THE MIDDLE ATLANTIC BIGHT

Anthony F. D'Agostino
Lieutenant Commander, United States Navy
B.G.S., University of Kansas, 1985

Submitted in partial fulfillment
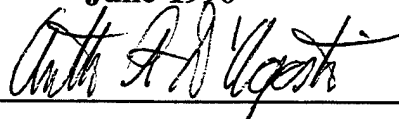of the requirements for the degree of

MASTER OF SCIENCE IN METEOROLOGY AND PHYSICAL OCEANOGRAPHY
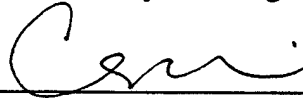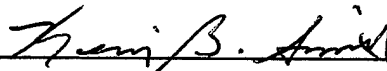
from the

NAVAL POSTGRADUATE SCHOOL

June 1996

Author: _____

Anthony F. D'Agostino
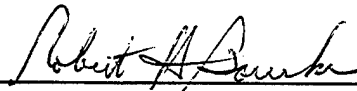
Approved by: _____

Ching-Sang Chiu, Thesis Advisor

_____

Kevin B. Smith, Co-Advisor

_____

Robert H. Bourke, Chairman
Department of Oceanography

iii

ABSTRACT

Under the sponsorship of the Office of Naval Research (ONR) PRIMER program, an integrated acoustic and oceanographic field experiment will be conducted jointly by the Naval Postgraduate School (NPS) and the Woods Hole Oceanographic Institution (WHOI) in the Middle Atlantic Bight (MAB) to study the propagation of sound from the continental slope to the continental shelf. In support of this field study the three-dimensional (3D) effects of the basic mean shelfbreak frontal thermal structure and sloping bathymetry on the planned tomography signal transmissions are modeled using ray methods. Both three-dimensional (3D) and two-dimensional (2D) ray paths and signal arrival structures for an upslope and cross-slope source-receiver geometry are simulated and compared. While the input sound speed field is from a previous summer-time hydrographic section, the input bathymetry is from a recently declassified U.S. Navy DBDB-0.5 data set. Significant 3D environmental effects are found in the modeled cross-slope transmissions, indicating that the physics of horizontal refraction and out-of-the-vertical-plane scattering will be required to properly analyze the acoustic measurements and to construct accurate tomographic maps.

TABLE OF CONTENTS

ACKNOWLEDGMENTS

I. INTRODUCTION

A. OCEAN ACOUSTIC TOMOGRAPHY

Tomographic methods are well documented in scientific literature. Historically it has been used by geophysicists to study the earths interior and by the medical community to study internal body structures. The word tomography comes from the Greek *tomos*, which means a cut, or section. Ocean acoustic tomography then is the study of the ocean by cutting or sectioning it with acoustic energy. Ocean acoustic tomography was originally proposed by Munk and Wunsch (1979) who presented methods for inverting acoustic travel time changes into ocean temperatures. They proposed the method to facilitate the monitoring of mesoscale processes in the deep ocean.

Tomography is an excellent tool for studying the ocean. Historically oceanographers have sampled the ocean using shore stations, shipboard, fixed platforms or sensor arrays, free and drifting buoys or satellite based sensors. The Nansen bottle, bathythermograph, CTD, current meter, and satellite image are all familiar tools to the oceanographer. Each of these tools have limitations that tomography can help overcome. Munk and Wunsch (1979) detail the advantages of tomography over traditional observation methods. Important considerations are: tomography allows the sampling of large ocean volumes quickly; a monitoring system could be permanently installed for long term, high resolution (spatial and temporal) data collection; fewer moorings are required than traditional monitoring systems; it provides information over the entire acoustic path, not just at the mooring site, as with traditional sensors.

Acoustic energy propagates through the ocean at a sound speed which is directly proportional to the ocean temperature, salinity and pressure. The ocean sound speeds are therefore related to the environment through which the acoustic waves pass. The knowledge of how sound speed changes affect the acoustic arrival structure (magnitude and travel time) is known as the *forward problem* in tomography. The forward problem establishes the physical relationship between the data and the

1

unknown, i.e., the ocean sound speed. The method of estimating sound speed from the data is known as the *inverse problem*.

Ocean acoustic tomography has traditionally been used in deep water. The adaptation of this acoustic technique from deep to shallow water has been addressed by Chiu et al. (1994, 1995, 1996). In August 1992 a coastal tomography experiment was conducted over the steep northwestern slope of the Bear Island Trough, about 100 km east of Bear Island. The experiment was designed to characterize and understand the dynamics of the Barents Sea Polar Front (BSPF) using acoustic tomography coupled with traditional physical oceanographic methods. The field experiment used a new tomography system using bottom-mounted sound sources and a vertical receiving array. In contrast to deep water propagation, the arrivals from the multi-paths in a shallow-water environment tend to overlap in time making it difficult to resolve the individual arrivals with omni-directional receivers. The vertical line array and beamforming techniques were used to overcome this difficulty. The experience gained from the BSPF experiment will be used and expanded upon during the upcoming Middle Atlantic Bight (MAB) field study.

As the U.S. Navy transitions operations from 'blue' to 'brown' water, it is increasingly difficult for the battlefield commander to quantify and categorize the complex littoral environment. In the coastal regime, environmental time and length scales are a tenth of their deep water counter parts; these compressed time and space scales make typification of the littoral regime exponentially more difficult. Acoustic tomography is the environmental scientists force multiplier. When properly employed it could enable the METOC (meteorology and oceanography) officer to quickly and accurately describe the ocean temperature and motion dynamics of the littoral ocean battle space.

B.   MIDDLE ATLANTIC BIGHT EXPERIMENT

Under the sponsorship of the Office of Naval Research (ONR), a summer and a winter experiment are scheduled to be carried out by the Naval Postgraduate School

(NPS) and Woods Hole Oceanographic Institution (WHOI) from July 1996 through August 1996 and from February 1997 through March 1997, respectively. The project is an integrated acoustic and oceanographic field study designed to examine sound propagation and ocean dynamics within the shelf break frontal zone which occurs near the transition from the continental shelf to the continental slope (Figure 1). Beardsley et al. (1994) have described 5 scientific objectives for the project:

1. To obtain a high resolution description of the spatial and temporal evolution of the shelfbreak front, and clarify the mechanisms by which eddies are formed and detached.

2. To determine the mean and seasonally varying circulation of the adjacent slope water, and characterize the mesoscale fluctuation in relation to shelfbreak processes.

3. To determine the effects of basic mean shelfbreak frontal thermal structure on the propagation of sound from the continental slope to the continental shelf.

4. To relate the temporal and spatial variability of acoustic propagation from the continental slope to the continental shelf with the associated variability of the shelfbreak front.

5. To make fully three dimensional tomographic images of the region of the shelfbreak front for use in physical oceanographic studies.

The modeling work presented in this thesis is in support of objectives 3 and 4. Specifically, this study examines the impact of three dimensional environmental effects on sound as it encounters the continental slope/shelf topography and the shelfbreak front, using a 3D ray-based acoustic propagation model.

C.   THESIS OBJECTIVES AND APPROACH

The objective of this thesis is to gain some apriori knowledge on how the fundamental shelfbreak frontal thermal structure and sloping bathymetry affect the propagation of sound from the continental slope to the continental shelf through modeling studies.
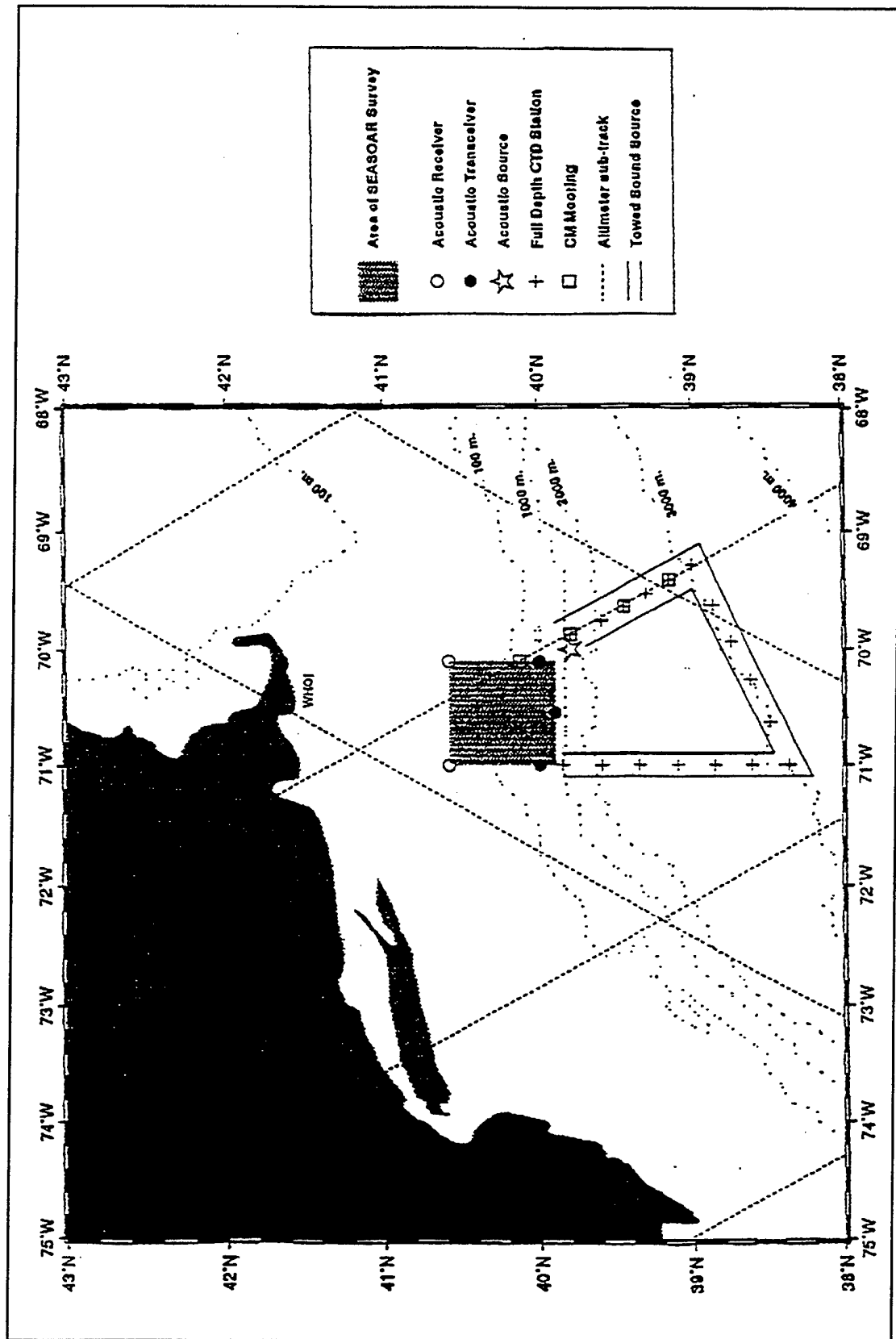
Figure 1 Middle-Atlantic Bight experimental area and configuration (From Beardsley et al. (1994)).

4

Specifically, the arrival structure of two of the planned 400-Hz tomography signal transmissions within the MAB experiment area are synthesized using both 2D and 3D ray modeling methods. The 2D and 3D calculations are then compared in an effort to quantify the significance of the 3D environmental effects. In addition, the synthesized beam signals are analyzed to provide information on the resolvability of the vertical receiving arrays.

The synthesis of the ray arrival structure is accomplished using the Hamiltonian Acoustic Raytracing Program for the Ocean (HARPO). Input to HARPO is a mathematical ocean environment developed from a previous cross-front hydrographic section in the experiment area and digital bathymetric data base (DBDB) bathymetry from the Naval Oceanographic Office (NAVO).

D.   THESIS OUTLINE

The remainder of the this thesis consists of three chapters. Chapter II describes the acoustic modeling process. Chapter III discusses the modeling results including comparisons of the 2D and 3D solutions and an analysis of resolvability. In Chapter IV conclusions are presented.

II. DESCRIPTION OF APPROACH

A. ENVIRONMENTAL MODELING

1. Bathymetry

The input bottom bathymetry model was developed based on the NAVO DBDB-0.5 data set. The DBDB-0.5 global data set is a classified (SECRET) bathymetry data set which contains bathymetric information for many areas of the worlds oceans and seas. Subsets of the DBDB-0.5 database are being systematically declassified for geographic areas which are no longer considered sensitive. Previous acoustic modeling efforts for the MAB experiment have used the DBDB-5 database. Acoustic modeling using the DBDB-0.5 database represents a two order of magnitude increase in the resolution of the input bathymetric field. Figure 2 displays the data set provided by NAVO.

Initial raytracing indicated a need to remove the fine structures in the DBDB-0.5 data that resulted in numerically unstable raypaths. An 8th order Butterworth digital filter was thus applied to the DBDB-0.5 data to establish a slightly smoother bathymetry for which numerical instabilities were eliminated.

2. Sound Speed

The input sound speed field for this study was developed by Chiu (1995) based on a summer hydrographic section obtained by Gawarkiewicz (1995). The representativeness of this sound speed model was investigated using available historical bathythermographic data for the region from NAVO. The NAVO Master Oceanographic Observation Data Set (MOODS) contains a total of 151 BT profiles for the month of July between 1913 and 1993 for the region. The 151 BT profiles were converted to sound speed profiles using the Medwin equation shown in Clay and Medwin (1977).

The 151 sound speed profiles were then analyzed for the mean location of the front and the envelope of gradients in the mean frontal zone. The frontal location and gradients in the input sound speed model are highly consistent with those in MOODS,
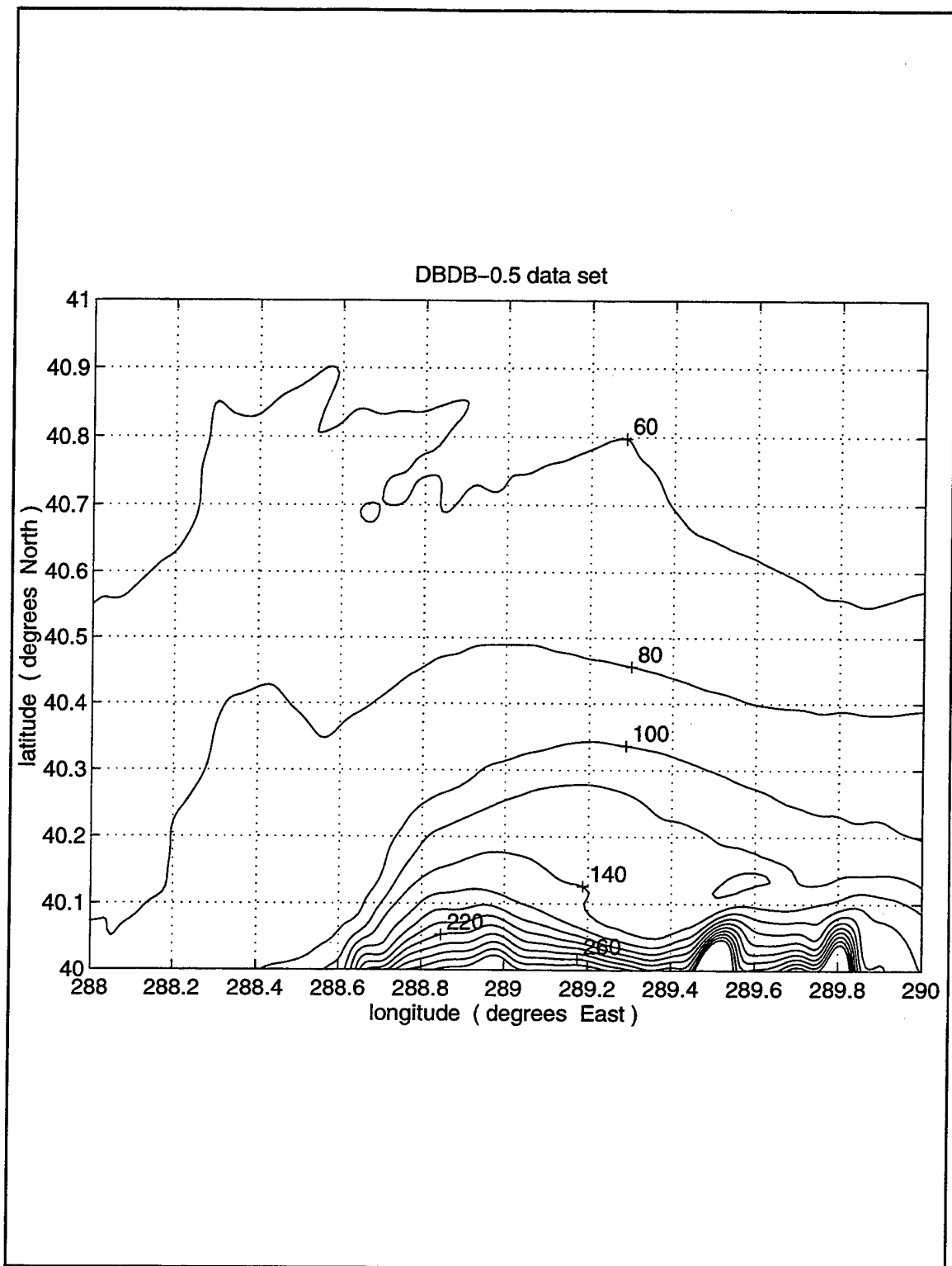
7

Figure 2 The DBDB-0.5 data set for the experimental region provided by the Naval Oceanographic Office (units in meters).

confirming the representativeness of the modeled ocean.

The modeled ocean consists of five identical latitudinal sections of sound speed profiles. The latitudinal sections have a longitudinal increment of 0.125°. Each section consists of 10 profiles spaced 5 km apart. Splines are then applied to create a smooth, continuous 3D ocean model. Figure 3 displays a cross section of the modeled ocean.

B. ACOUSTIC MODELING TRACKS

The simulated source-receiver geometry is shown in Figure 4. The geometry defines two distinct acoustic tracks, one running up-slope and the other cross-slope.

1. North-South Track

The North-South (NS) acoustic modeling track runs directly up-slope with the source located at 40.00°N-289.65°E and receiver at 40.32°N-289.65°E. The distance between the source and the receiver is 35 km. The source is placed at a depth of 242 m in 262 m of water. The receiver is a full-column vertical hydrophone array placed in 90 m of water.

2. North-West Track

The North-West (NW) acoustic track crosses the slope obliquely. The corresponding full-column vertical hydrophone array is located at 40.32°N-289.25°E, 50 km from the source. The array is in 104 m of water.

C. ACOUSTIC MODELING

1. Raytracing

Ray theory was used for this modeling study of the planned acoustic transmissions in the MAB experiment. All 2D and 3D rays were traced using HARPO. HARPO is fully three dimensional in its physics. Therefore the rays have full freedom to refract and reflect as they interact with the sound speed gradients and boundaries. The input ocean model is required to have a continuous sound speed field and a continuous bathymetry. This continuity was achieved using an interpolating interface to the gridded data developed by Chiu et al. (1994). For calculation of the 2D rays the line-of-sight sound speed slice and bathymetry was first replicated.

9

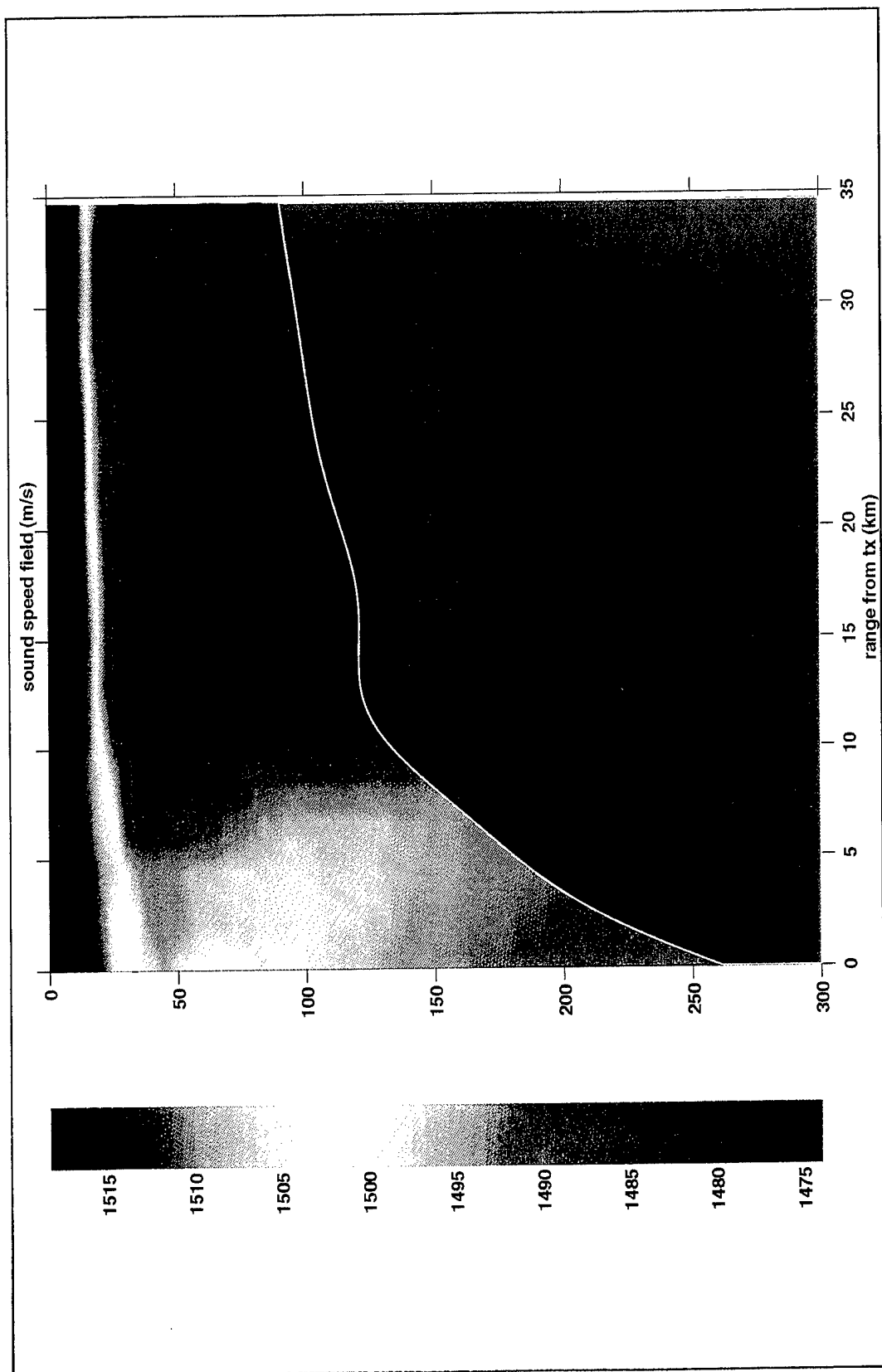**Figure 3** Modeled sound speed field along with the modeled bathymetry along the NS up-slope track. 0 km is the location of the source. Depth in meters.
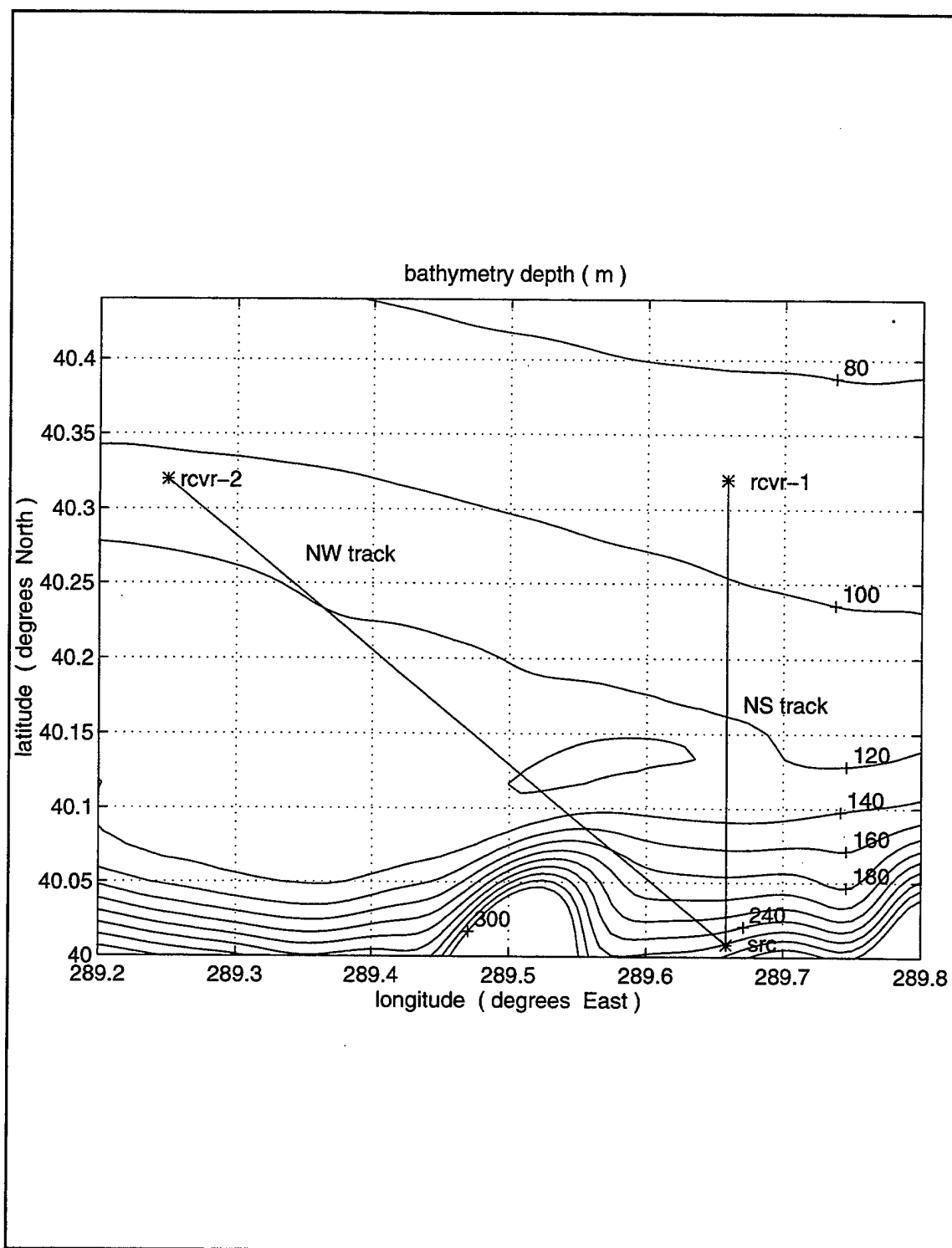
Figure 4 Placements of the 400-Hz tomography source (**src**) and two vertical hydrophone arrays in relation to the bottom bathymetry. **rcvr-1** is the location of the hydrophone array for the NS track, **rcvr-2** is the location of the hydrophone array for the NW track.

11

The replicates were then placed in parallel in the ocean model to null the azimuthal gradients.

HARPO traces rays based on the integration of a differential form of Fermat's principle (Jones et al., 1986). The differential equations are known as Hamilton's equations and have the following form in cartesian coordinates:

$$\frac{\partial x_i}{\partial \tau} = \frac{\partial H}{\partial k_i} \quad ; \quad \frac{\partial k_i}{\partial \tau} = -\frac{\partial H}{\partial x_i} \, , \, i=1, 2, 3 \tag{1}$$

where τ is a parameter whose physical meaning depends on how the Hamiltonian, H, is defined, k_i are the wave-number components, and x_i are the coordinates of a point on the ray path. For acoustic waves in the ocean, the Hamiltonian is defined as:

$$H(x_i \, , \, k_i) = \omega^2 - c^2 \, (x_i) \, (k^2) = 0 \tag{2}$$

where ω is the angular wave frequency and c (x_i) is the sound-speed field (Jones et al., 1986). Initial conditions for x_i and k_i are directly related to the launch elevation and azimuth angles.

a. NS Track Raytracing

Initial coarse-resolution HARPO model runs were conducted to bracket suitable ranges of launch angles for the final high-resolution runs. For the 2D case, rays were initially traced with launch elevation angles between -25° to +25° in 1° increments. This coarse-resolution run revealed that rays with launch angles less than -7° and greater than +7° have ray angles incident at the bottom exceeding the critical angle (~25°) on the shelf. Thus, sound propagating along these steep rays would suffer significant bottom loss before reaching the receiver. Neglecting these high-loss raypaths, the final high-resolution set was traced between -7° and +7° at a resolution of 0.01°.

Example vertical geometries of the high-resolution 2D rays are shown in Figure 5. Notice the dramatic differences in the ray traces caused by only small changes in the launch angles. Because the ray interacts with the steep bottom, slight change in the launch angle can direct the ray into markedly different sound speed regions of the frontal boundary which causes the ray path to change dramatically. The chaotic behavior which these rays exhibit was first observed in underwater acoustics by Palmer et al. in 1988, and further studied by Brown et al. (1991) and Smith et al. (1992). Chaotic rays are characterized by their "extreme sensitivity" to initial conditions. Ray chaos is not an issue in the traditional modeling of range-independent environments but complicates the interpolation of ray processes in complex range dependent environments such as the MAB.

For the 3D case it was also necessary to bracket the range of azimuthal launch angles, since this case allows for horizontal refraction. Coarse-resolution 3D ray fans with elevation angles between -7° and +7° were launched at azimuth angles between 359° and 001° in 0.05° increments. It was found that ray fans launched at azimuths between 359.95° and 000.05° bracketed the receiver location. Figure 6 displays the horizontal ray geometries of the two limiting coarse-resolution ray fans with launch azimuths of 359.95° and 000.05° , respectively. The final high-resolution 3D ray set was thus traced from -7° to +7° in elevation angle with an increment of 0.01° and from 359.95° to 000.05° in azimuth angle with an increment of 0.025°.

Figure 7 shows the dependence of the horizontal distance from the receiver to a ray along the wavefront that intersects the receiver on launch elevation and azimuthal angles. This dependence is central to the determination of the horizontal eigenrays.

b. NW Track Raytracing

The same procedure involving an initial coarse-resolution run was also used to bracket the initial elevation and azimuthal angles for the NW track. For this case, the limiting launch elevation angles were -7° and +7° and the limit azimuthal
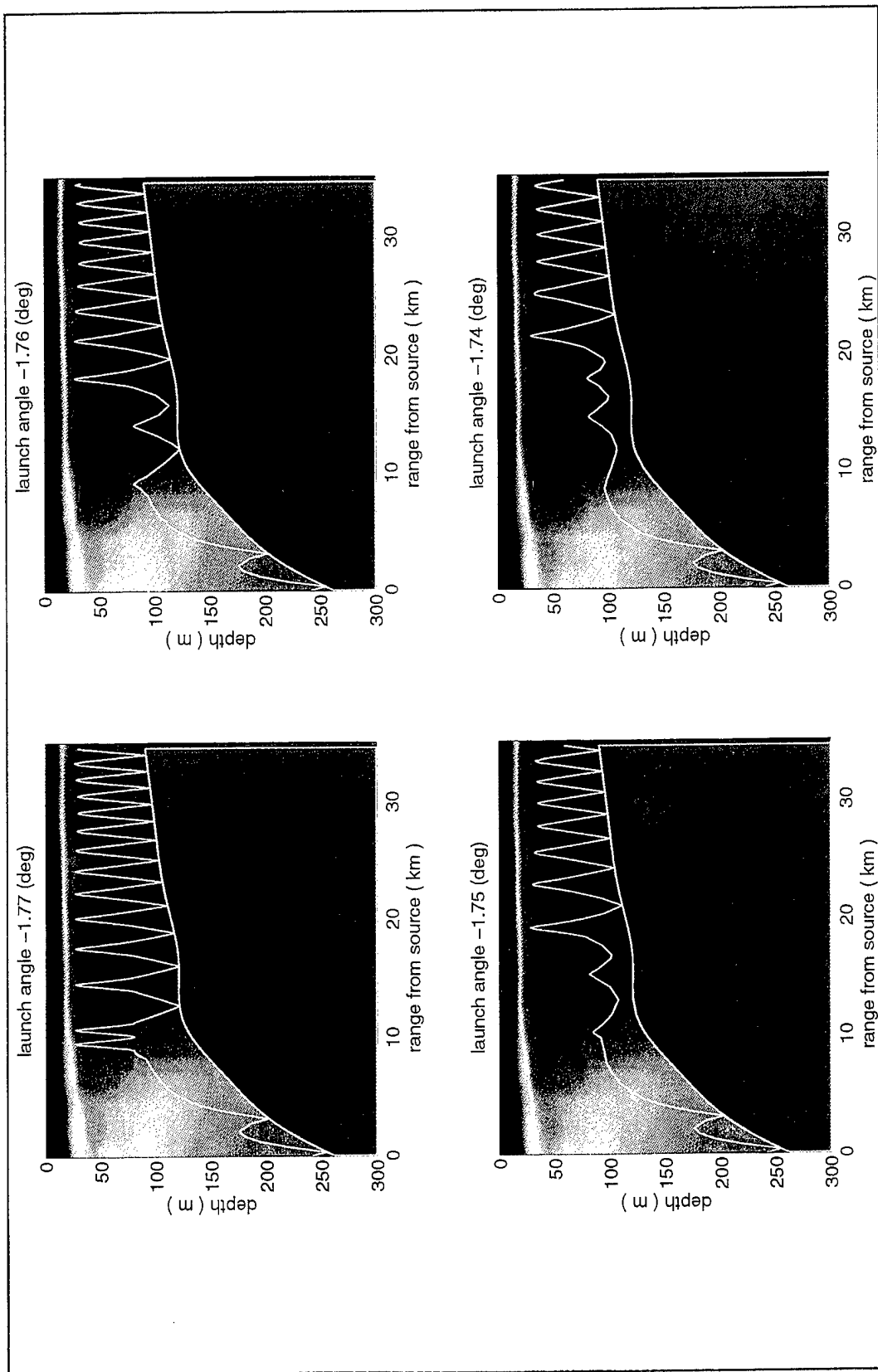
Figure 5 Geometries of some of the up-slope 2D rays with small initial angles, showing significant sensitivity to small changes in the launch angle.
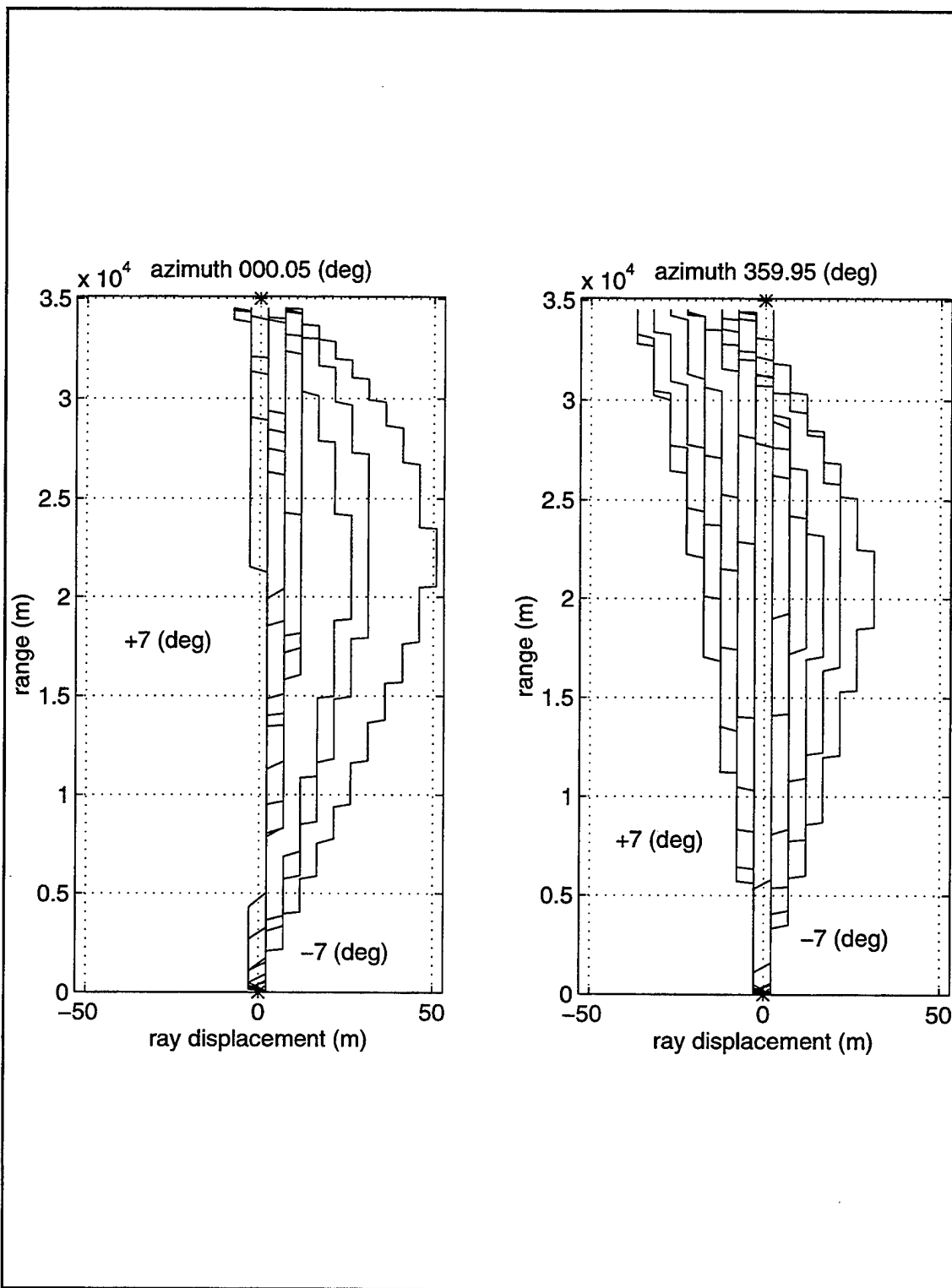
Figure 6 Horizontal geometries of two vertical ray fans with launched azimuthal angles of 000.05 degrees (left panel) and 359.95 degrees (right panel), respectively, computed from the course-resolution 3D-NS run.

15

Figure 7 The dependence of horizontal distance to the ray from the receiver along the intersecting wavefront on launch elevation angle and azimuth angle for the 3D-NS case.

angles were 314.90° and 315.10°, respectively. The final, high-resolution ray set has a resolution of 0.01° in the elevation angle and a resolution of 0.05° in the azimuthal angle.

2.   Eigenray Determination

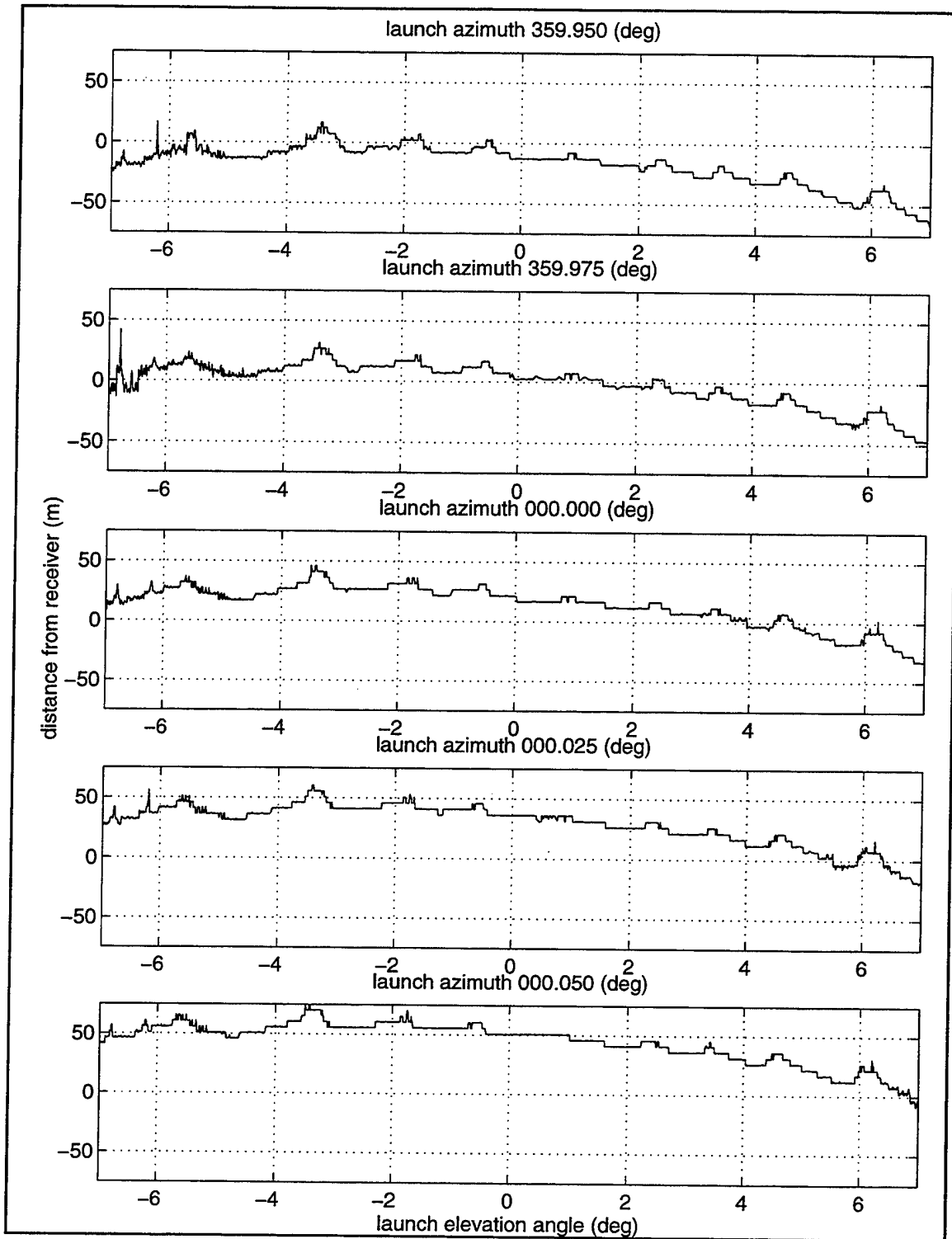Eigenrays are rays which connect the acoustic sound source to the receiver. HARPO does not search for eigenrays; this search was performed using external algorithms developed by Chiu (1995). Briefly, for each of the ray launch elevation angles, the horizontal eigenray was first determined by finding the root of the along-wavefront horizontal distance mismatch versus azimuthal angle curve. Using the set of horizontal eigenrays, the eigenrays at each hydrophone depth was determined by finding the roots of the depth mismatch versus elevation angle curve. The algorithms then go on to compute the eigenray pressure magnitudes, phases and travel times including the effects of the boundary reflections, ray turning and raytube spreading. Figure 8 is a plan view of the eigenray geometries showing the azimuthal deviations from the line-of-sight as a function of range for all the 3D eigenrays for both the NS and NW cases. The NS track bisects the ocean front and bathymetry at approximately right angles and thus the azimuthal deviations are minimal (less than 50 m). The NW track however bisects the ocean front and the bathymetry along a diagonal and is clearly affected by 3D effects from both the ocean frontal structure and bathymetry. The horizontal refraction of the steep eigenrays is controlled by the bathymetry which curved the eigenrays to the right. The small-angle eigenrays are curved to the left by the frontal structure. The intermediate-angle eigenrays thus experience competitive horizontal refraction effects.

3.   Arrival Structure Synthesis

The sound sources to be deployed during the MAB experiment have a full bandwidth of 100-Hz centered at 400-Hz. They will transmit phase-encoded pseudo-random m-sequences which correspond to 10 millisecond pulses after matched filtering at the receiver. Therefore, the synthesis of the complex envelope (i.e., matched filter output) of the omnidirectional arrival structure can be accomplished by summing all

17
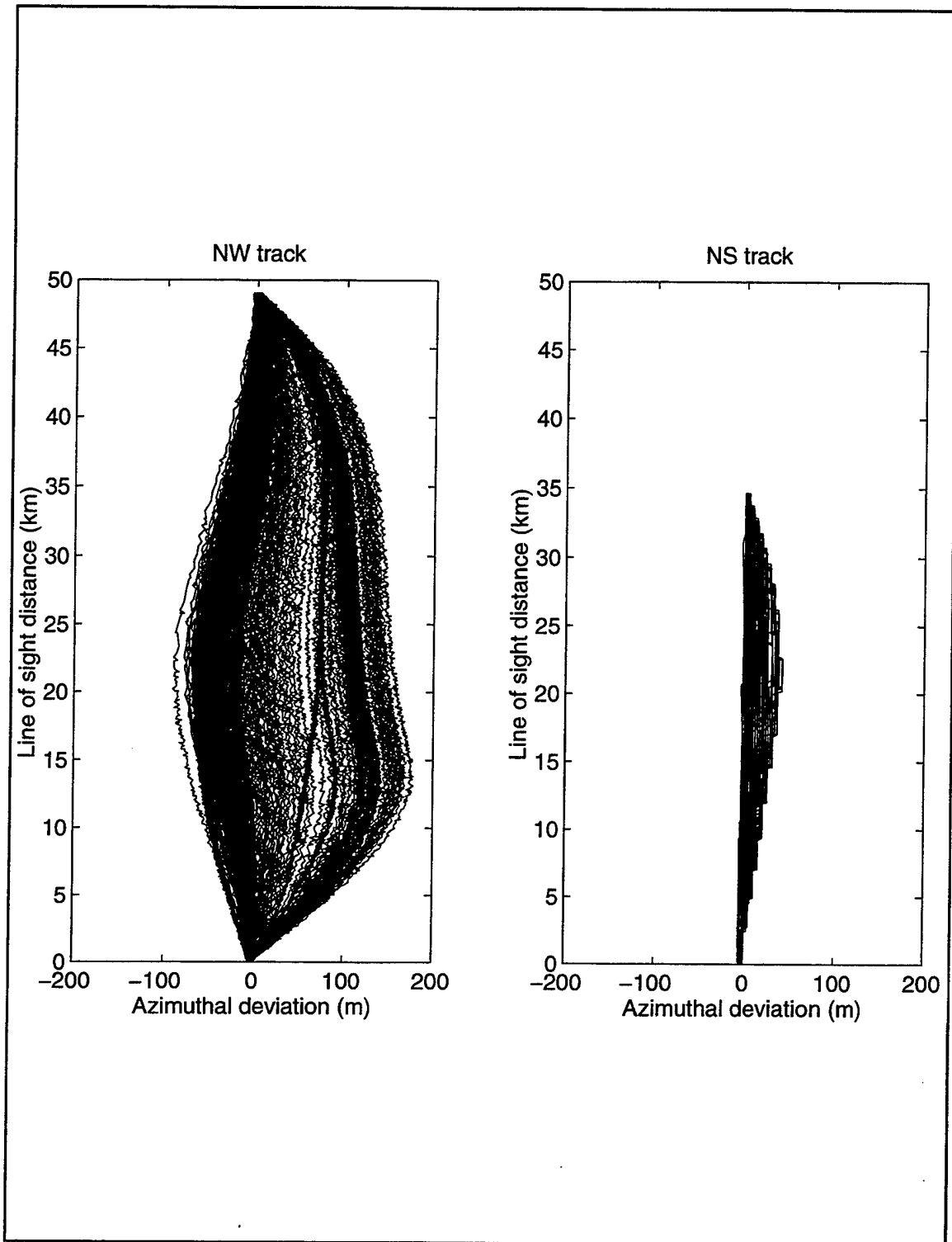
Figure 8 Plan view of the geometries of all eigenrays, showing azimuthal deviation versus range for the 3D NS (right panel) and NW (left panel) cases. The NW case shows significant horizontal refraction, with a maximum azimuthal deviation of 180 meters from the line-of sight caused by 3D effects.

the individual eigenray contributions as magnitude-scaled, phase-shifted and time-delayed complex envelope of the source pulse:

$$\check{r}\,(t) \,=\, \sum_{i=1}^{N} \, a_i \, \check{S}\,(t - t_i) \tag{3}$$

where $\check{S}\,(t)$ represents the complex envelope of the source pulse, $\check{r}\,(t)$ the complex envelope of the processed received signal, a_i modification in amplitude and phase, t_i time delay and N the number of eigenrays.

III. RESULTS AND DISCUSSION

A. 2D VERSUS 3D

1. North-South Track

The top panel of Figure 9 shows the synthesized arrival structure (magnitude only) as perceived by an omni-directional element of the vertical hydrophone array for the NS track. The element is located at a depth of 50 m and the arrival structures of both the 2D and 3D solutions are displayed. For this track, the 2D and 3D arrival-structure solutions are in good agreement with each other, both containing four relatively strong arrivals followed by approximately a dozen weak ones. The timing (or phasing) of these arrivals, strong or weak, also match extremely well between the 2D and 3D cases.

This strong similarity between the 2D and 3D solutions is further illustrated in Figure 10 where the arrival structures are displayed in significantly more detail, as a function of arrival time and angle. These time-angle arrival structures can be viewed as vertical array outputs. Visually, they reveal, beam-by-beam (i.e., at each arrival angle), close agreement between the 2D and 3D solutions for the NS track. This beam-by-beam agreement can be quantified by cross-correlating the complex envelopes of the beams of the 2D and 3D solutions. The results are displayed in Figure 11 as correlation peaks and lags as functions of beam angle. The beams were chosen to be approximately two-degrees wide for reasons to be explained later. Consistently high correlations of 0.8 and above and lags close to zero for most of the beams are evident.

In the context of ray acoustics, a definitive verification of the 2D approximation can be obtained by comparing the eigenray geometries. Since all the eigenrays are bottom interacting, the difference between the number of bottom bounces of the 2D and 3D eigenrays is an excellent indicator of resemblance. Figure 12 shows this difference for the NS track. The number of bottom bounces versus launch elevation angle for the 2D and 3D eigenrays are shown in the top and middle panels,
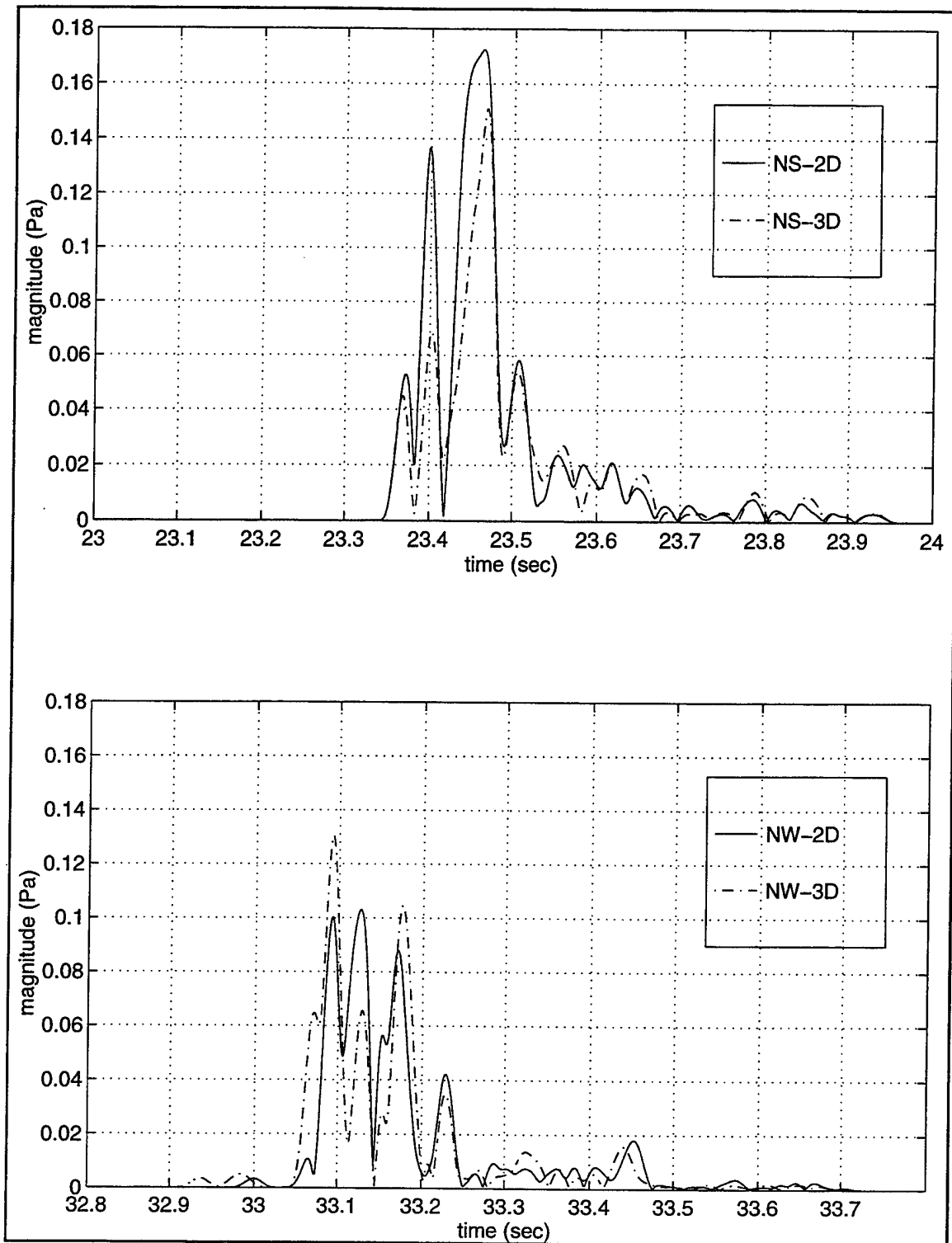
21

Figure 9 Omnidirectional arrival structure for the NS track (top) and for the NW track (bottom). The arrival structure is for a single hydrophone located at a depth of 50 meters. The solid line represents the arrival structure of the 2D solution and the dot-dashed line represents the arrival structure of the 3D solution.
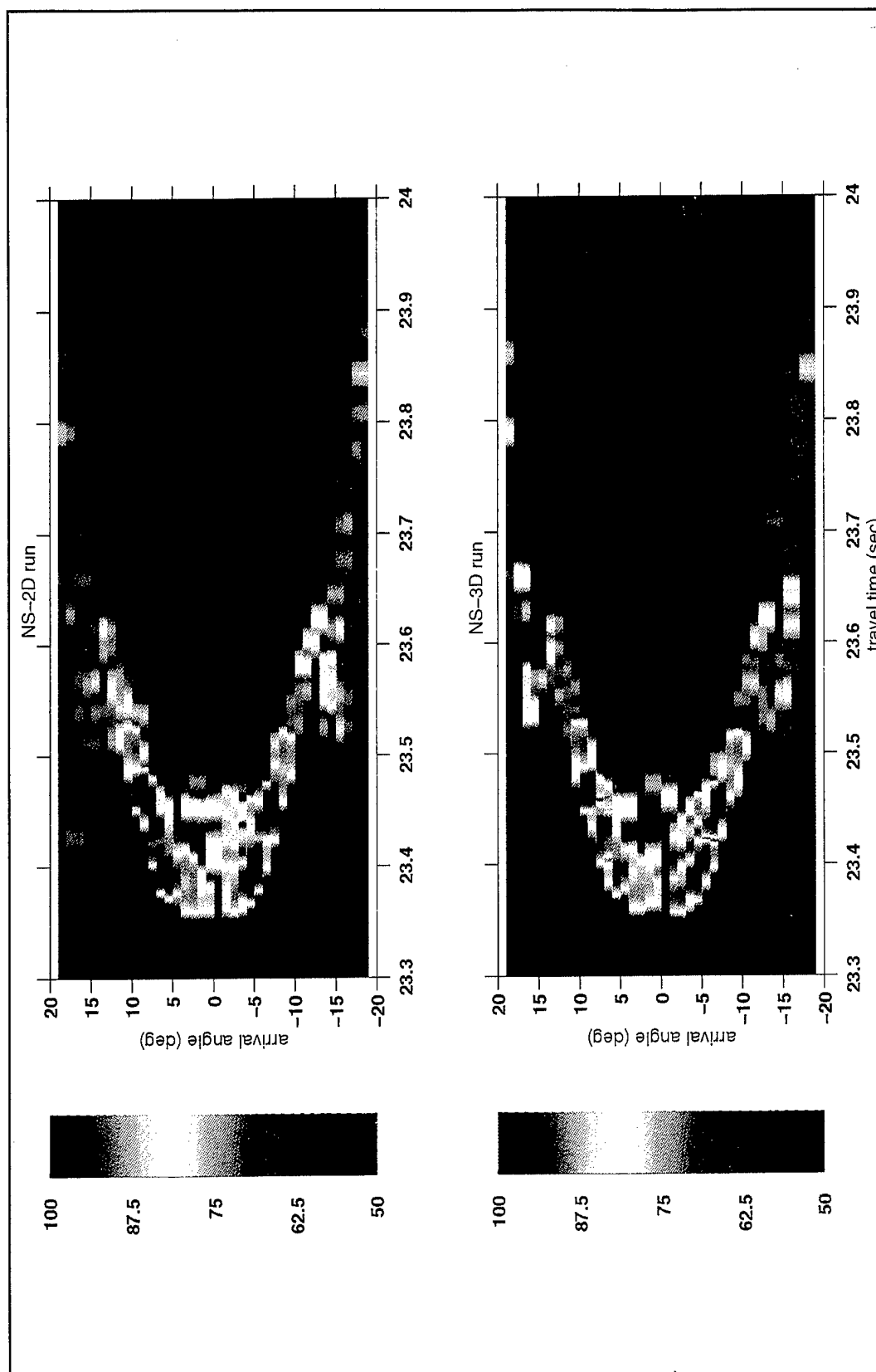
Figure 10 Arrival structure as a function of arrival time and angle for the NS cases. The 2D arrival structure solution is displayed in the top panel and the bottom panel shows the 3D counterpart. Colorbar units in decibels.

23

Figure 11 Peaks (top) and lags (bottom) of the cross-correlations of the 2D and 3D beam solutions for the NS track.

Figure 12 Number of bottom interactions versus launch angle for the 2D (top) and 3D (middle) eigenrays and their differences (bottom), for the NS track.

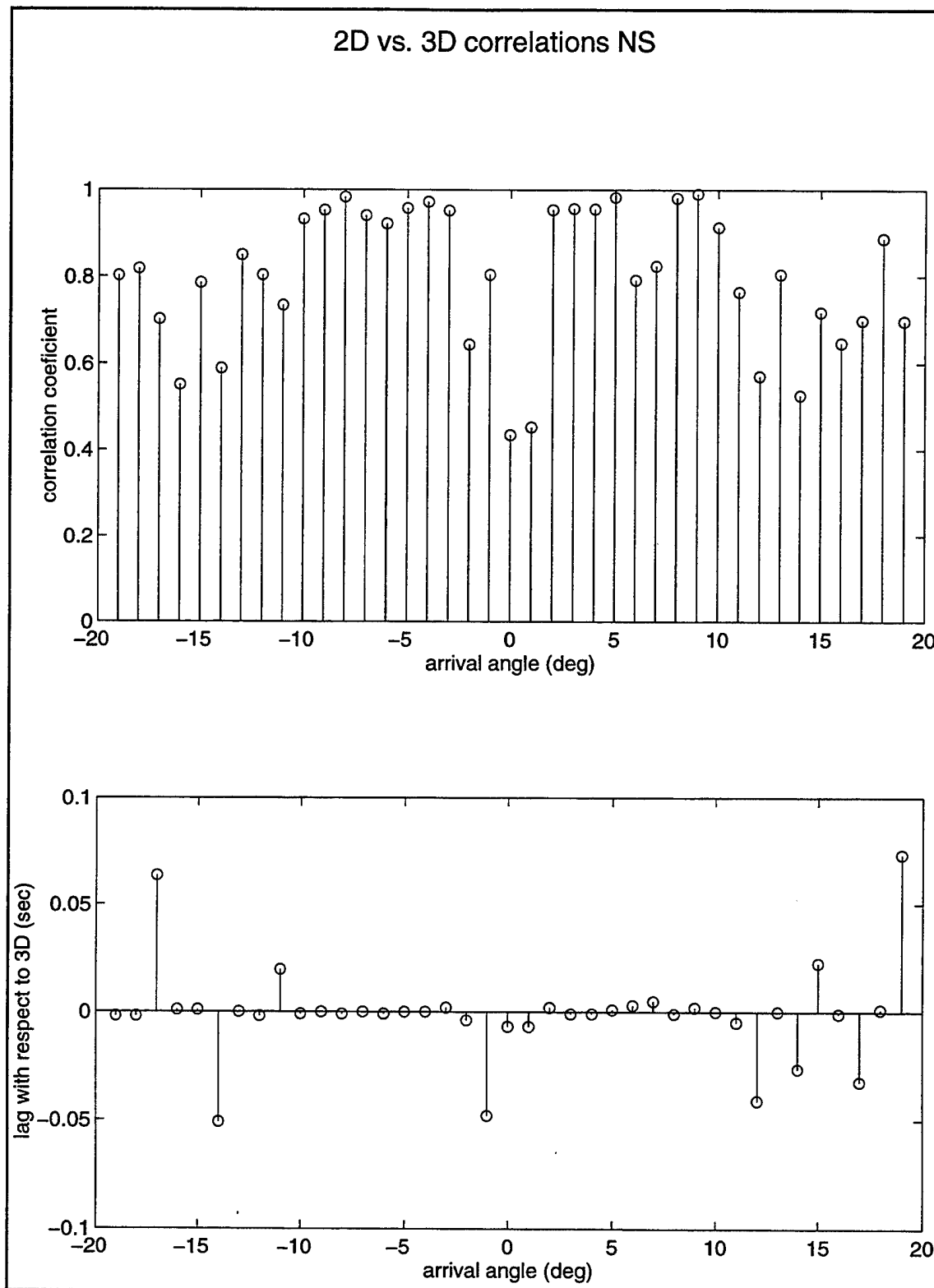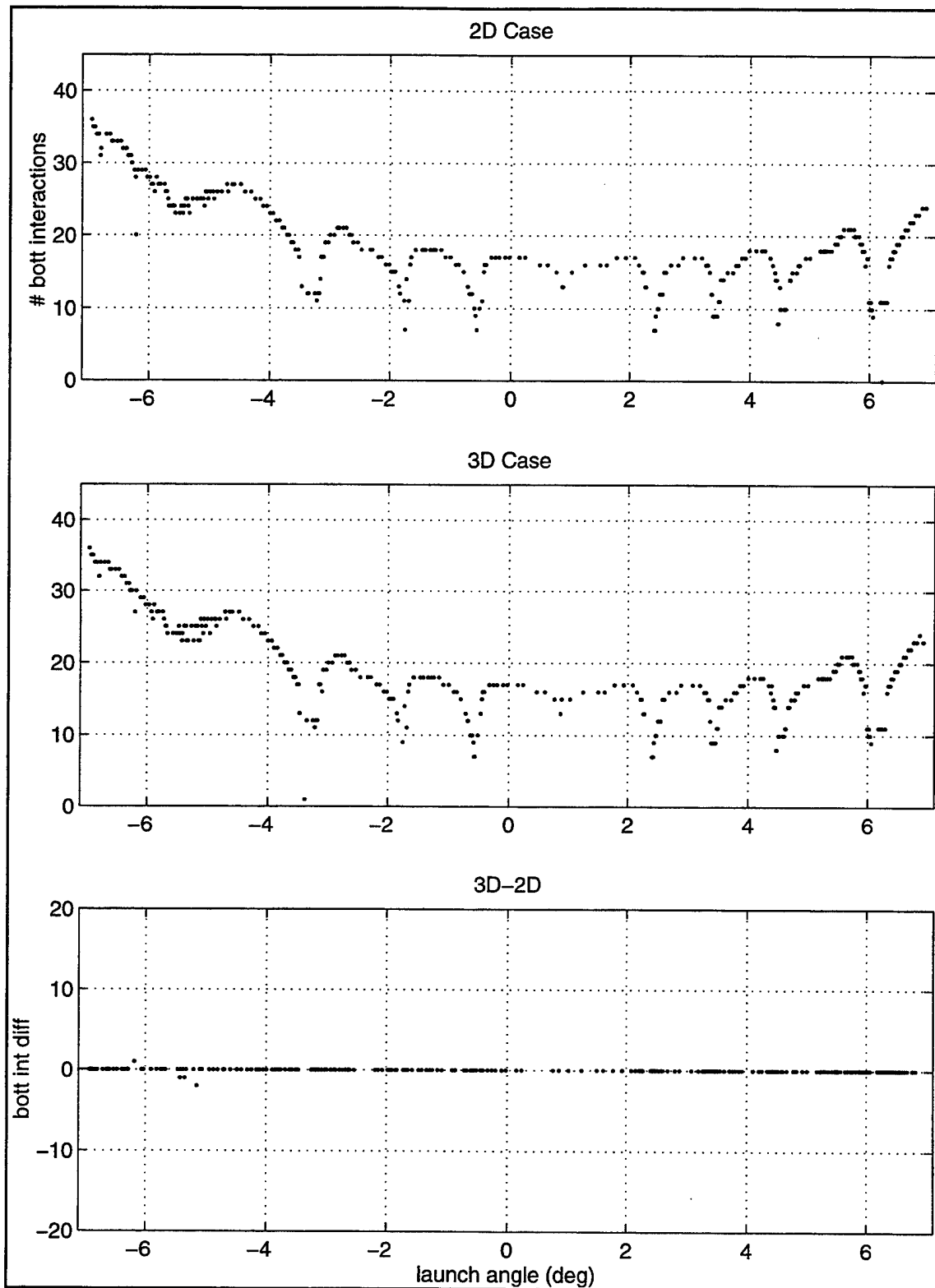while their differences are shown in the bottom panel. Without a doubt, the 2D and 3D eigenrays for the NS track are almost identical as indicated by the minimal differences. These good overall agreements, however, are anticipated as the NS track runs almost normal to the isobaths and the frontal boundary.

2. North-West Track

The 2D and 3D results paint a different picture for the NW track, indicating the inadequacy of the approximate 2D physics. In terms of the gross pattern, larger differences between the omni-directional arrival structures of the 2D and 3D solutions can be easily spotted from the bottom panel of Figure 9. The dissimilarities are more appreciable in the beams as can be seen in Figures 13 and 14.

In Figure 13, the time-angle arrival structures of the 2D and 3D solutions for the NW track are displayed, showing considerable differences between the two structures. For example, the strongest arrivals (i.e., red spots in the figure) in the 3D solution are more scattered in the time-angle surface and are not as tightly grouped as in the 2D solution. Comparison of the arrival patterns at a specific arrival angle (i.e., beam) reveal further differences. The peaks and lags of the cross-correlations between the complex envelopes of the 2D and 3D beam solutions for the NW track are shown in Figure 14, revealing a low correlation of 0.6 on the average, as well as unacceptably large lags for most of the beams.

More importantly, the geometries of the 2D and 3D eigenrays for the NW track are almost entirely different. The number of bottom bounces as a function of launch elevation angle for the 2D and 3D eigenrays and the differences in the number of bounces are shown in Figure 15. The differences can be as large as 15 bounces.

B. RESOLVABILITY

1. North-South Track

The synthesized omni-directional arrival structure at the hydrophone at the 50-m depth for the NS-track is shown in Figure 16 again. But the current plot also includes the eigenray arrival times and relative amplitudes that make up the overall pattern. The temporal distribution of the eigenray "sticks" scaled by the relative
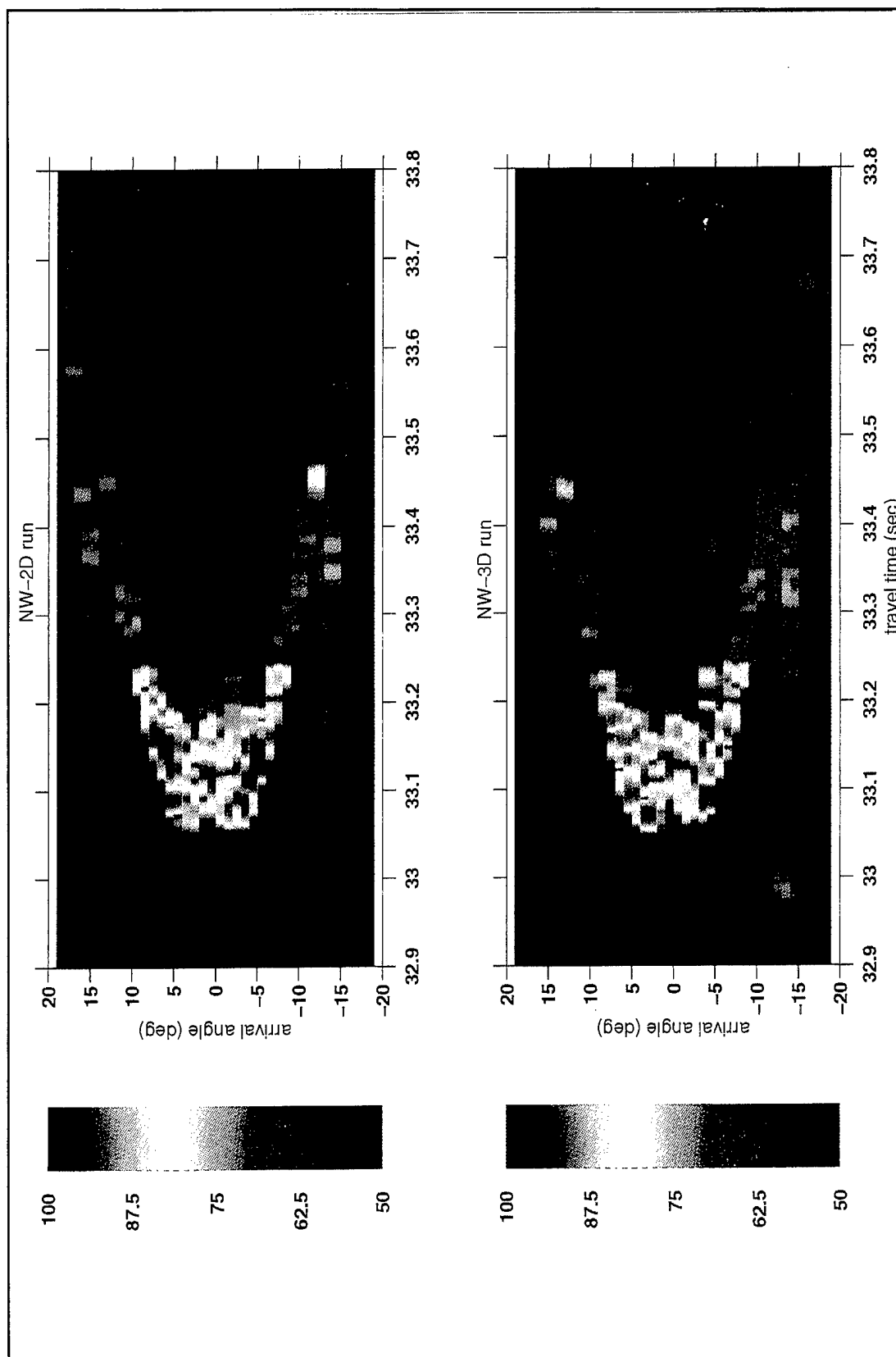
Figure 13 Same as Figure 10 but, for the NW track.
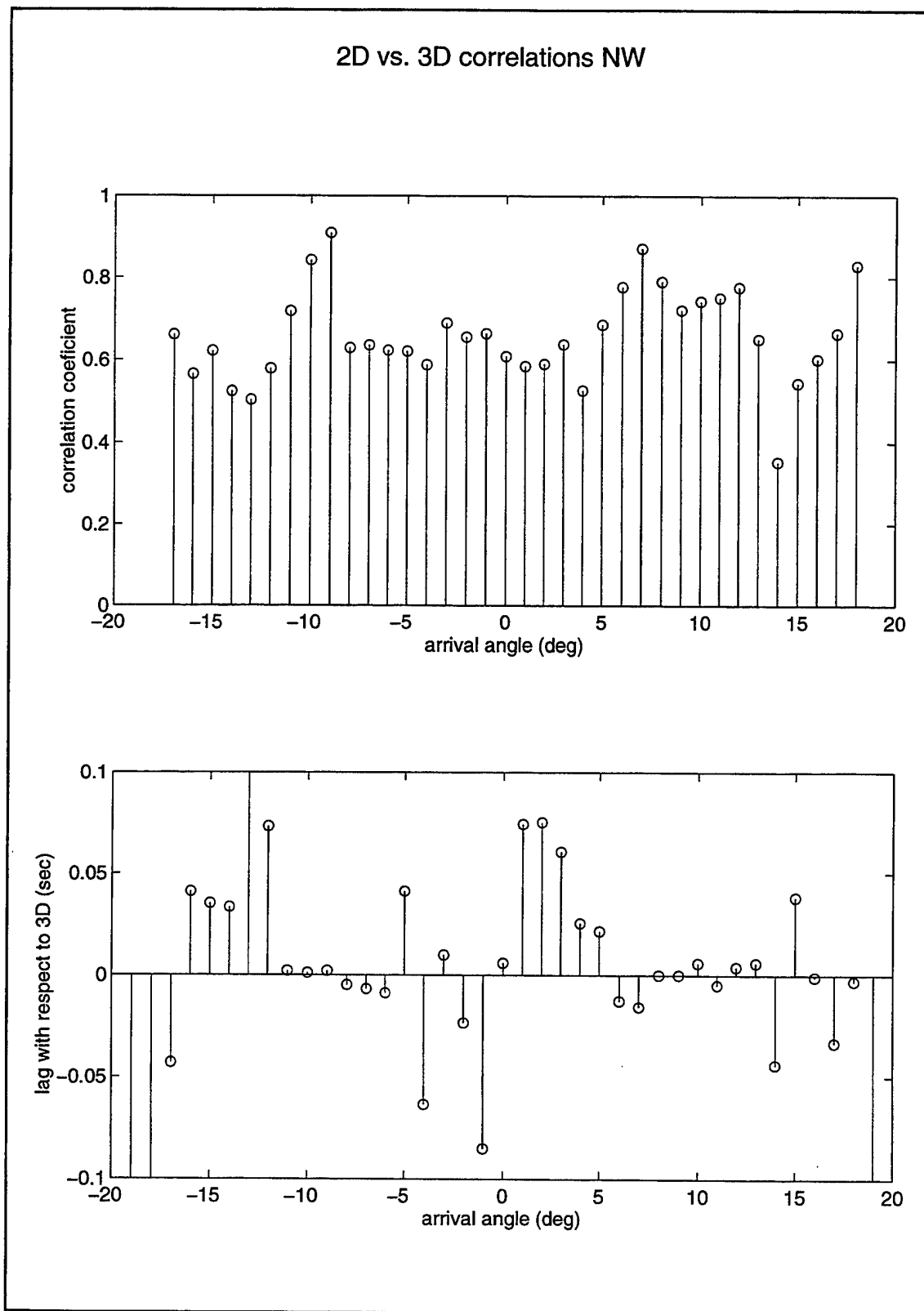
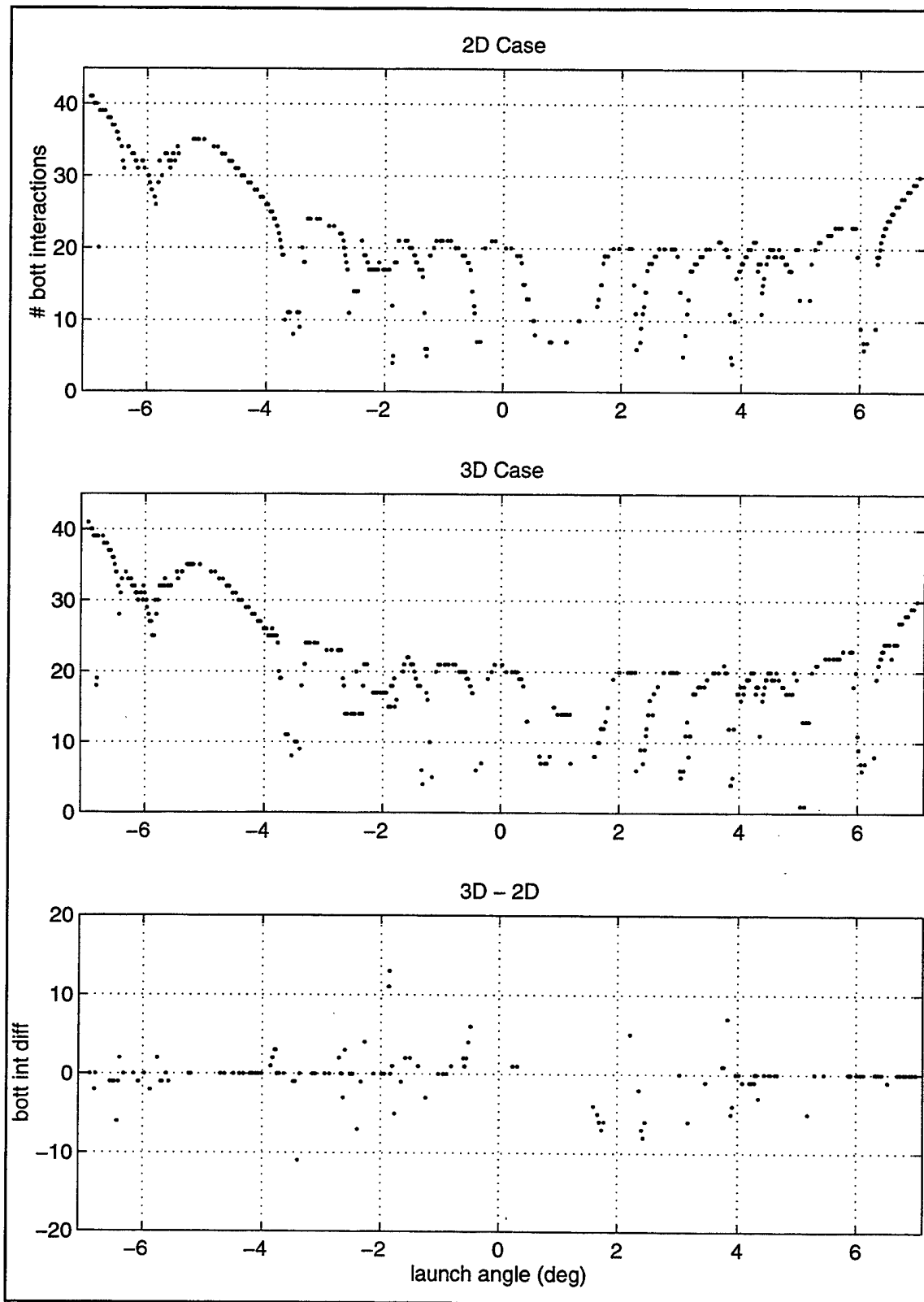**Figure 14** Same as Figure 11 but, for the NW track.

28

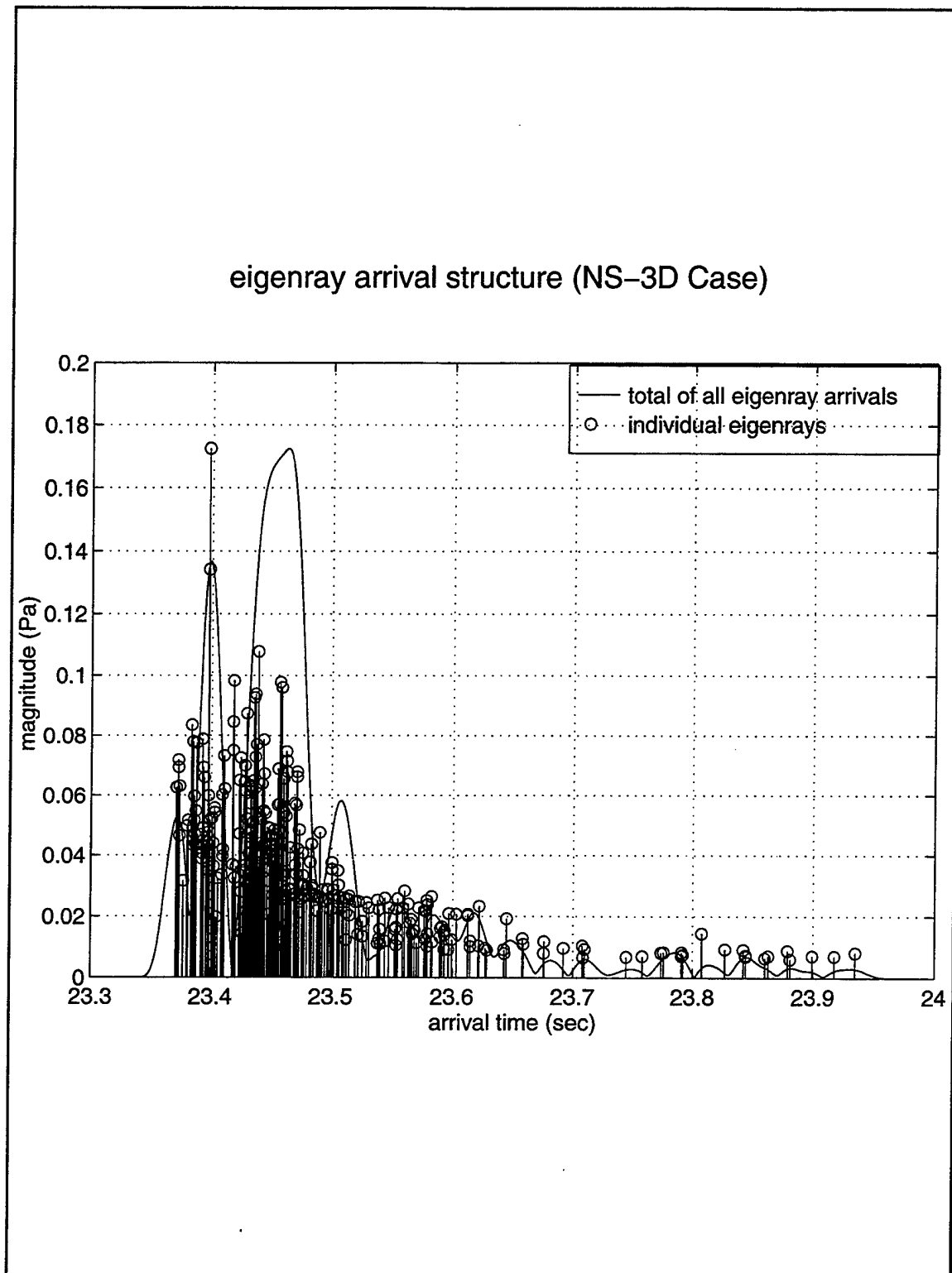**Figure 15** Same as Figure 12 but, for the NW track.

Figure 16 Same as top panel of Figure 9 except that the eigenray travel times and relative amplitudes are explicitly plotted as "sticks".

30

amplitudes can be thought of as the reception of the emission of an ideal pulse with infinite bandwidth. Thus, in order for individual pulses to be resolvable, the sticks must be separated by the operational width of the pulse, which is 10 milliseconds for the MAB sound source under consideration. Clearly, none of the individual arrivals can be resolved in time by a single phone and the use of beamforming arrays is crucial.

The beam-pattern of the full-column arrays for the MAB experiment for a look direction of zero-degree grazing is plotted in Figure 17. With 16 equally-spaced elements the beamwidth is approximately 2 degrees and depends weakly on look direction. To facilitate the resolution analysis, the corresponding beam arrival structure is replotted in Figure 18. But, unlike the previous plot (bottom panel of Figure 10), the amplitude information is now withheld and the widths of the individual arrivals are explicitly shown as circles with diameters of 10 milliseconds. Non-overlapping circles in the diagram thus represent resolvable individual eigenpaths. It is seen that the small-angle eigenrays with arrival angles between ±2 degrees and a majority of the steeper eigenrays with arrival angles larger than +10° or smaller than -10° are resolvable by the vertical array in this NS track. It is worth mentioning that, although some of the steeper-angle arrivals come in as overlapping pairs, they can still be incorporated in the mapping of the ocean, since those pairs did go through pretty much the same ocean volumes. As an example, the ray geometries of one such pair are shown in Figure 19.

2. North-West Track

Figure 20 shows the beam arrival structure for the NW track. The situation here is quite similar to the NS case, with some resolvable arrivals at low-grazing angles between ±2 degrees and more resolvable arrivals beyond ±10 degrees.

31
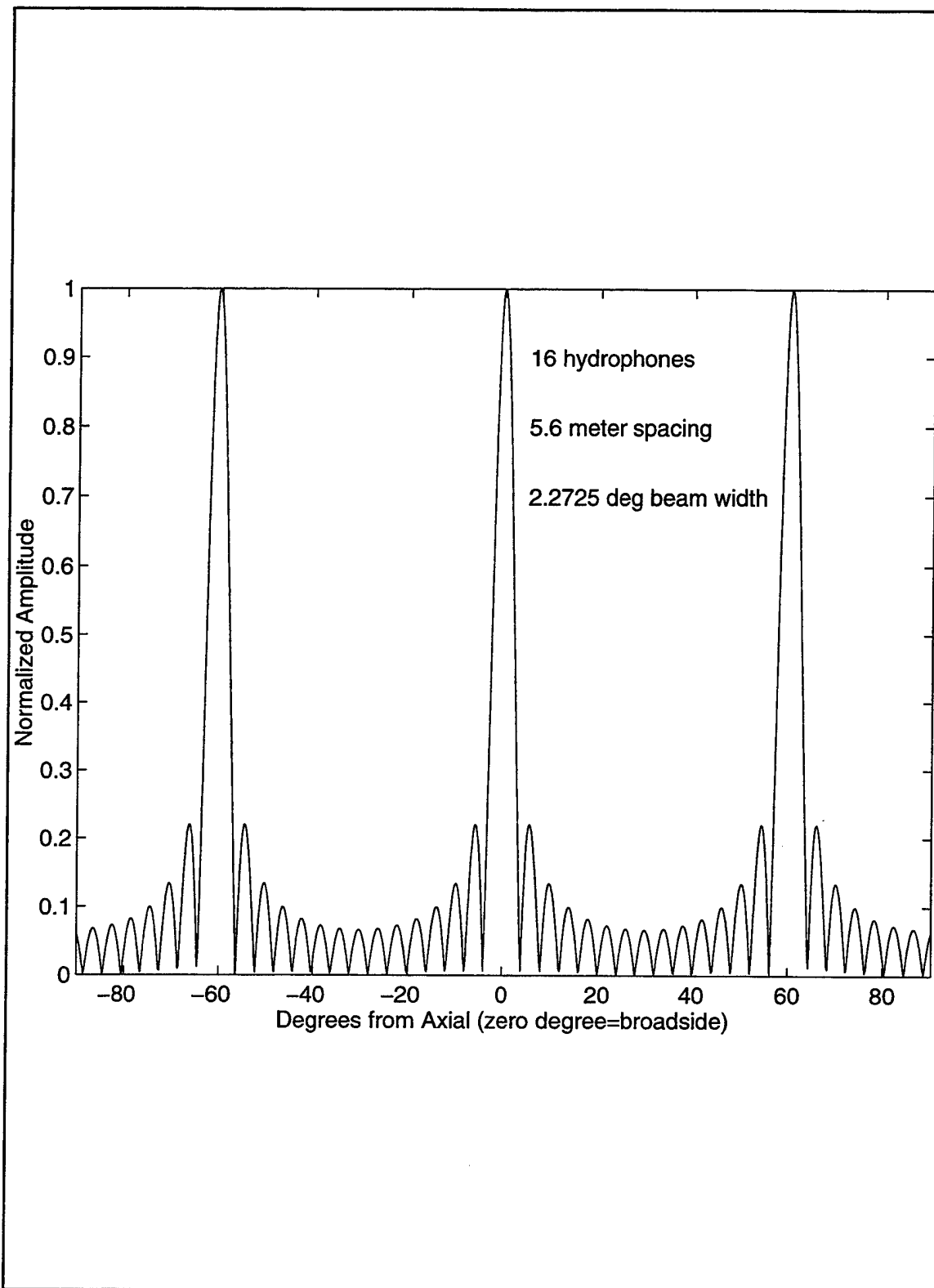
Figure 17 Theoretical beam pattern for the full-column vertical hydrophone array for a look angle of zero degree grazing at 400-Hz.

32
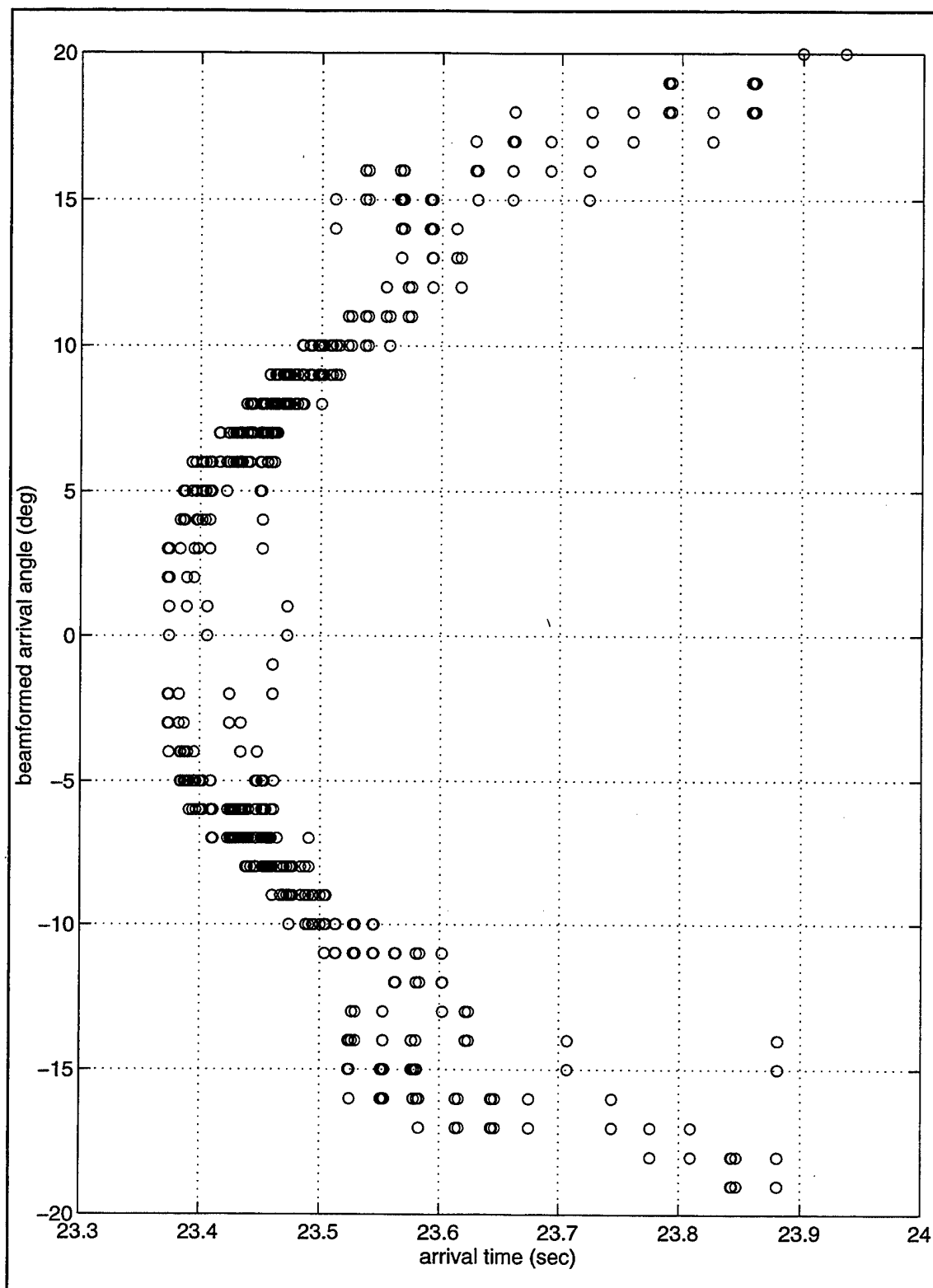
Figure 18 Beam arrival structure for the NS track. Amplitude information is omitted but, pulse width is shown by circles with 10 millisecond diameters.

Figure 19 The ray geometries associated with a pair of arrivals overlapping in time showing that the corresponding paths go through similar ocean volumes.

Figure 20 Same as Figure 18 but, for the NW track.

35

IV. CONCLUSIONS

As part of the upcoming Mid Atlantic Bight Experiment, 400-Hz tomography signals will be transmitted from three sound sources moored on the continental slope to two vertical receiving arrays moored on the continental shelf. Using a 3D, ray-based acous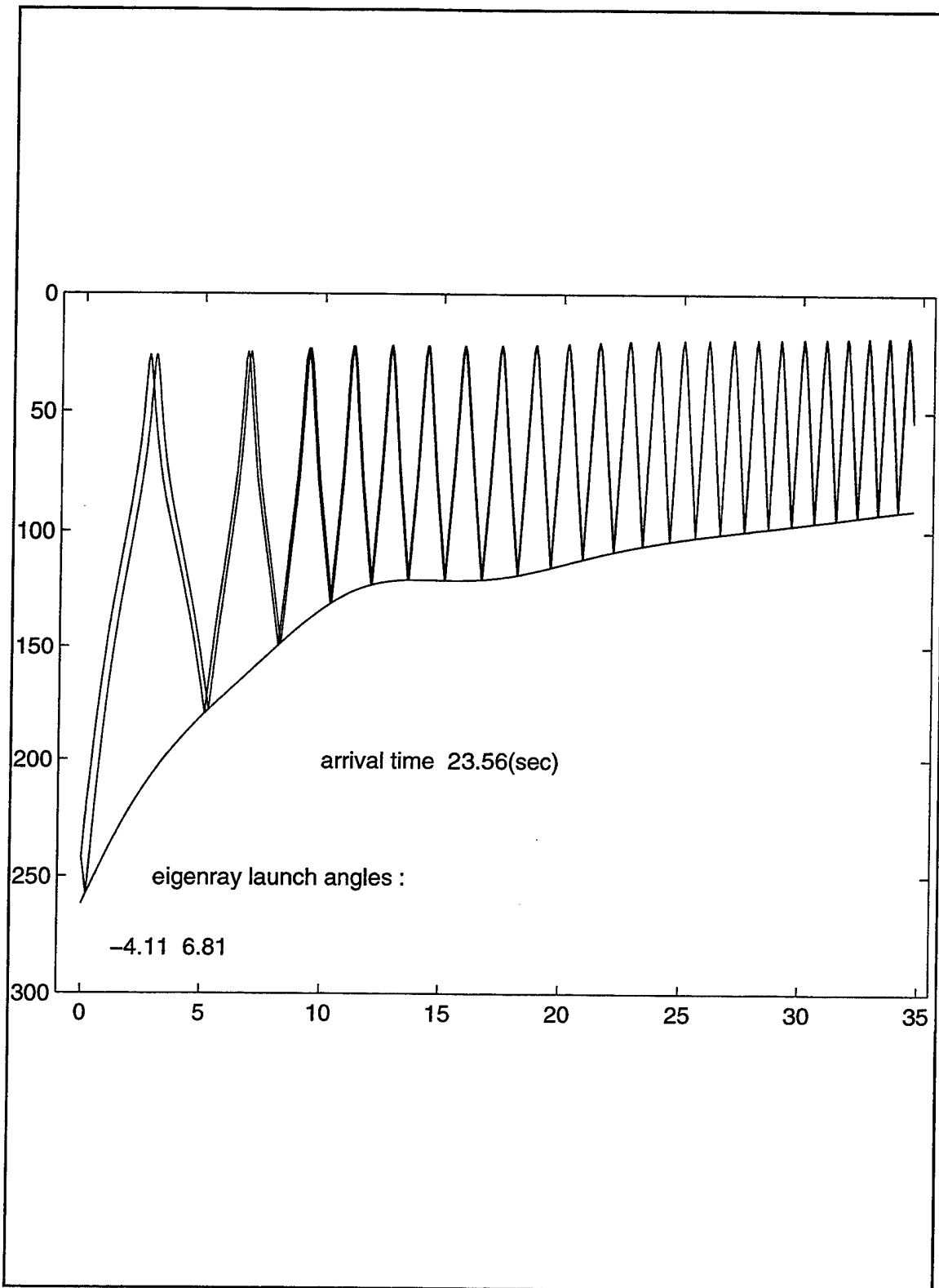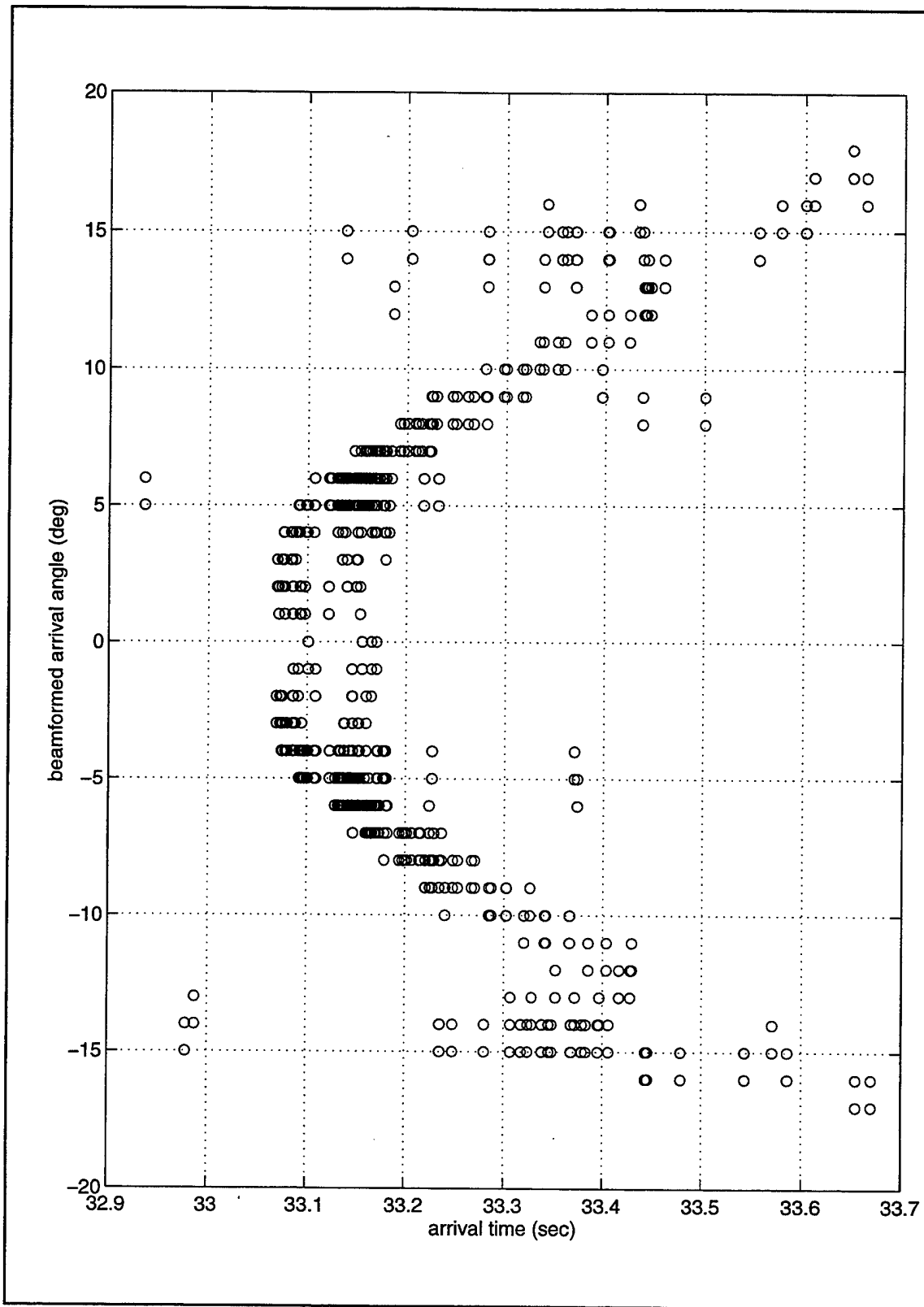tic model, the objectives of this thesis were to assess the significance of the 3D effects of the sloping bathymetry and shelfbreak frontal structure on two of the planned transmissions and to examine the resolvability of the ray arrivals for use in the tomographic mapping of the shelf-break frontal structure.

The simulated source-receiver geometry provided an upslope acoustic track with a NS orientation and a cross-slope acoustic track with a NW orientation. While the NS track was perpendicular to the frontal boundary, the NW track crossed the front obliquely. The quantification of the 3D environmental effects involved comparisons between the 2D and 3D ray solutions. The resolvability issues were addressed through the analysis of the synthesized beam data. Major conclusions are:

1. For the NS track, the differences between the 2D and 3D results are small, revealing the adequacy of using approximate 2D propagation physics in the analysis of the up-slope and directly cross-front transmissions. For this track, the omni-directional arrival structures, beam arrival structures as well as eigenray geometries of the 2D and 3D calculations are in close agreement.

2. For the NW track, significant differences between the 2D and 3D solutions are found. The arrival structures of the 2D and 3D solutions are quite dissimilar. In addition to having low correlations and large lags between the beams in the 2D solution and the 3D solution, the 2D and 3D eigenray geometries are entirely different. Significant horizontal refraction, with a maximum azimuthal deviation of 180 m from the line-of-sight, is also found along this track. These results strongly indicate that, for the NW oblique track, the inclusion of the 3D effects will be required to properly model and analyze the acoustic data and to construct tomographic maps.

3. The synthesized beam arrival structures associated with both the NS and

NW tracks suggest that some of the small-angle eigenrays with arrival angles between ±2 degrees and a majority of the steeper eigenrays with arrival angles larger than +10 degrees or smaller than -10 degrees are resolvable by vertical arrays. Thus, the ray arrivals coming in at these angles should be useful for the mapping of the shelfbreak frontal structure in conjunction with resolvable modal arrivals (Chiu et al., 1994, 1995, 1996).

LIST OF REFERENCES

Beardsley, R.C., K.H. Brink, J. Candela, M.J. Caruso, C.-S. Chiu, G.G. Gawarkiewicz, K.A. Kelly, J.F. Lynch, J.H. Miller and R. Pickart, "Sound Propagation from the Continental Slope to the Continental Shelf: An Integrated Acoustic and Oceanographic Field Study," Research proposal submitted to the Office of Naval Research, 1994.

Brown, M.G., Tappert, F.D., Goni, G. and K. B. Smith, "Chaos in underwater acoustics," in *Ocean Variability and Acoustic Propagation*, edited by J. Potter and A. Warn-Varnas, Kluwere Academic, Dordrecht, 1991.

Chiu, C.-S., J.H. Miller, J.F. Lynch , "Forward coupled-mode propagation modeling for coastal acoustic tomography," *Journal of the Acoustical Society of America*, Vol. 99, pp. 793-802, 1996.

Chiu, C.-S., J.H. Miller, W.W. Denner and J.F. Lynch , "Forward modeling of the Barents Sea tomography vertical line array data and inversion highlights," in *Full Field Inversion Methods in Ocean and Seismic Acoustics*, edited by O. Diachok, A. Caiti, P. Gerstoft, and H. Schmidt (Kluwer Academic, Dordrecht, 1995), pp. 237-248, 1995.

Chiu, C.-S., J.H. Miller and J.F. Lynch , "Inverse Techniques for Coastal Acoustic Tomography," *Journal of Geophysical Research*, Vol. 92:C7, pp. 6886-6902, 1994.

Chiu, C.-S., Department of Oceanography, Naval Postgraduate School, Monterey, CA, Personal Communication, 1995.

Clay, C.S. and H. Medwin, *Acoustical Oceanography*, John Wiley and Sons, New York, 1977.

Jones, R.M., J. P. Riley and T.M. Georges, *"HARPO: A Versatile Three-Dimensional Hamiltonian Ray Tracing Program for Acoustic Waves in an Ocean with Irregular Bottom,"* Wave Propagation Laboratory, National Oceanic and Atmospheric Administration, Boulder, CO, 457 pp., 1986.

Gawarkiewicz, Department of Applied Ocean Physics and Engineering Woods Hole Oceanographic Institution, Woods Hole, MA 02543 Personal Communication, 1995.

Munk, W., P. Worcester and C. Wunsch, *"Ocean Acoustic Tomography,"* Cambridge University Press, New York, 1995.

Munk, W. and C. Wunsch, "Ocean Acoustic Tomography: A Scheme for Large Scale Monitoring," *Deep Sea Research*, Vol. 26A, pp. 123-161, 1979.

Palmer, D.R., M.G. Brown, F.D. Tappert and H.F. Bezdek, "Classical chaos in nonseperable wave propagation problems," *Goephysical Research Letters*, Vol. 15, pp. 569-572, 1988.

Robinson, A.R., and D. Lee, *Oceanography and Acoustics: Prediction and Propagation Models*, American Institute of Physics, Woodbury, New York, 1994.

Smith, K.B., M.G. Brown and F.D. Tappert, "Ray Chaos in Underwater Acoustics," *The Journal of the Acoustical Society of America*, Vol. 91:4, pp. 1939-1949, 1992.

INITIAL DISTRIBUTION LIST

1. Defense Technical Information Center   2
    8725 John J. Kingman Rd., STE 0944
    Ft. Belvoir, VA 22060-6218

2. Dudley Knox Library   2
    Naval Postgraduate School
    411 Dyer Rd.
    Monterey, CA 93943-5101

3. Professor Robert H. Bourke (Code OC/BO)   1
    Department of Oceanography
    Naval Postgraduate School
    Monterey, CA 93943-5000

4. Professor Ching-Sang Chiu (Code OC/CI)   4
    Department of Oceanography
    Naval Postgraduate School
    Monterey, CA 93943-5000

5. LCDR Anthony F. D'Agostino, USN   4
    579 B Wilkes Lane
    Monterey, CA 93940

6. Dr. Ellen Livingston (Code 321OA)   1
    Office of Naval Research
    800 North Quincy Street
    Arlington, VA 22217

7. Dr. James F. Lynch   1
    Department of Applied Ocean Physics and Engineering
    Woods Hole Oceanographic Institution
    Woods Hole, MA 02543

8. Dr. James H. Miller   1
    Department of Ocean Engineering
    211 Sheets Building
    Narragansett, RI 02882-1197

9. Dr. Steve Ramp (Code 322PO)   1
    Office of Naval Research
    800 North Quincy Street
    Arlington, VA 22217

10. Dr. Jeff Simmen (Code 321OA)   1
    Office of Naval Research
    800 North Quincy Street
    Arlington, VA 22217

11. Professor Kevin B. Smith (Code PH/SK)   1
    Department of Physics
    Naval Postgraduate School
    Monterey, CA 93943-5101